SYNTHETIC BIOMIMETIC COMPLEXES OF THE OXYGEN EVLOLVING COMPLEX OF PHOTOSYSTEM II AS WATER OXIDATION CATALYSTS FOR ENERGY APPLICATIONS

A Thesis

by

MICHAEL A. KAYNE

BS, Texas A&M University-Corpus Christi, 2018

Submitted in Partial Fulfillment of the Requirements for the Degree of

MASTER OF SCIENCE

in

CHEMISTRY

Texas A&M University-Corpus Christi
Corpus Christi, Texas

May 2020

May 2020

SYNTHETIC BIOMIMETIC COMPLEXES OF THE OXYGEN EVOLVING COMPLEX OF PHOTOSYSTEM II AS WATER OXIDATION CATALYSTS FOR ENERGY APPLICATIONS

A Thesis

by

MICHAEL A. KAYNE

This thesis meets the standards for scope and quality of
Texas A&M University-Corpus Christi and is hereby approved.

Jai Prakash, PhD
Chair

Patrick Larkin, PhD
Committee Member

Hussain Abdulla, PhD
Committee Member

May 2020

ABSTRACT

Fossil fuels are the major source of greenhouse gasses. There is a global effort to find a replacement fuel. Renewable energy is a primary focus and already provides a substantial portion of energy demand. Among them is molecular hydrogen (H_2). This is due to its combustion and fuel cell product being water as well as its use as energy storage. Further, H_2 can be obtained in a green and renewable way through electrolysis of water. However, Clean H_2 production is currently expensive, and catalysts are one solution to help bring the costs down. Development of catalysts for this purpose have the added benefit of elucidating complex redox reactions involved in photosynthesis and the formation of the O-O bond.

Direct inspiration from nature has led to the development of proposed water oxidation catalysts. These are synthetic metal-ligand (organometallic) complexes attempting to mimic the structure and functionality of the oxygen evolving complex (OEC) found in photosystem II. The goal is to mimic this unique portion of photosynthesis. This is done by producing ligands capable of binding three to four metal atoms and testing each complexes' ability to perform the redox reactions associated with splitting water into hydrogen and oxygen.

Ligands are designed and produced that utilized terminal pyridine groups to chelate three or four metal atoms. These ligands are complexed with the manganese atom inspired by nature as well as the less expensive and more abundant iron atom. The iron complex is spectroscopically compared to that of the manganese. In the future these organometallic complexes will be reacted with calcium and oxidizing agents and undergo further spectroscopic, redox and electrochemical tests.

DEDICATION

STEM subjects are possibly the most difficult disciplines to study. Anyone who finds a passion in the sciences will need help and inspiration to truly succeed. I would like to thank all the professors that helped me stay focused. Thank you to my Mentor, Dr. Jai Prakash, for giving me the most valuable apprenticeship I have ever known. And an eternity of gratitude and appreciation to my family for supporting me on this journey.

This is dedicated to everyone who is willing to be there for and support someone walking down a very difficult and elusive path.

ACKNOWLEDGEMENTS

The scope of this project is global. It reaches deep into the past and extends far into the future. I acknowledge and appreciate every scientist, university and company within whom I relied upon for the knowledge to pursue this venture. It is my hope that the small contribution of this thesis will also be a reliable source for future work.

Texas A&M University Corpus Christi, and the professors that call it home, were critical to the completion of my master's thesis. It is within them that I have found guidance.

Dr. Fari Billiot, Dr. Eugene Billiot, Dr. Jordan Alexander, Dr. Riccardo Mozzachiodi, Dr. Timothy Causgrove, Dr. Cesar Marquez, Dr. Jim Silliman, Dr. Shreyashi Ganguly, Dr. Narendra Narayana and many more.

Nikolai Kraiouchkine always gave me his full attention when I had a question or needed help with the instrumentation on campus.

Dr. Patrick Larkin was key in my understanding of biological systems and photosynthesis, and he always dedicated an incredible amount of time and focus when it came to my work.

Dr. Hussain Abdullah helped me to understand a vast array of spectroscopy and spectroscopic techniques that constitute the blossoming of a chemist's superpowers.

Dr. Jai Prakash, my mentor and guide, took me under his wing and patiently walked me through the first stage of my chemical career. He is a beautiful person and I hope I have gained the knowledge and experience he wanted me to have. Above all, it is his uncanny attitude toward the chemical sciences that I wish to have absorbed.

Thank You

TABLE OF CONTENTS

INTRODUCTION

Fossil fuel has been used since before the common era.[1] Its uses are as broad as the time frame of its use, ranging from fire to luxury goods and beyond. In 1597 Andreas Libavius, in his work Alchemia[2], proposed a theory surrounding the creation of fossil fuels stating that they were from dead plant matter exposed to millions of years of heat and pressure beneath the Earth's crust.[3] In 1759 (1773 2nd edition, English translation) Caspar Neumann, in his work *The Chemical Works of Caspar Neumann*, first mentions the phrase 'fossil fuel'.[4] Today, it has multiple uses, but its main use is in energy applications.

There is a wide range of data sources pointing to different aspects of the exponentially increasing use of fossil fuels and what its use means or implies. Each with its own set of pathways that seems to multiply, or even turn in circles, as one quests for the right analytical approach. What matters is that many intelligent people are paying close attention, and that data is increasing as more and more countries come online. A powerful and reliable source of this information is the data collected by the U.S. Energy Information Administration (EIA) or its sources i.e. the United States Environmental Protection Agency (EPA) and the National Oceanic and Atmospheric Administration (NOAA). The EIA works internationally with the United Nations Framework Convention on Climate Change (UNFCCC). Further, a tool supported by these organizations that uses officially reported data is climatewatchdata.org; an amazing stand-alone tool with access to the cited and graphical data and its sources. Authors of cited material that have not drawn their data from the EIA, EPA, UNFCCC, NOAA or climatewatchdata.org have been funded by credible institutions like the National Science Foundation (NSF) and/or an accredited university. Due to the extremely dynamic nature of this data and its various sources, the reader is encouraged to seek further confirmation of cited material and stay up to date.

The industrial revolution and the interconnected global economy are a direct result of increased use of fossil fuel (coal first and then oil).[5] The advancements during the first and second industrial revolutions caused rapid population growth[6-9] and cut out human dependence on the unpredictable elements such as the wind and water currents harnessed by our ancestors. Humans could circumnavigate the globe without horses or the need to rely on the wind.[10] These revolutions changed the planet, but the burning of fossil fuel had yet to make its debut as a major player in the global climate.

As the world clashed and connected, more discoveries were made that would indirectly affect fossil fuel's contribution. Two chemists, Fritz Haber and Carl Bosch, gave the world easy access to ammonia when they developed a chemical process that converted atmospheric N_2 to NH_3, now called the Haber-Bosch Process.[11] Ironically, the Haber-Bosch Process is cited as the detonator of the population explosion.[12-13] This is due to the increased ammonia available for fertilizer and thus an increase in food. The abundance of food led to a dramatic global population boom.[14] The multiplying human population steadily increased the weight of fossil fuel's contribution leading to a tipping point. The use of fossil fuel, now coupled with human population growth, became a global climate changing force. In fact, in the 1950s the human population began to produce a net CO_2 gain.[15] This simply means there is more CO_2 being released into the atmosphere than all of Earth's processes as a whole can absorb.

Carbon dioxide is not the only, nor the most effective, greenhouse gas. There are others, such as; methane, nitrous oxide and fluorinated gases. However, CO_2 makes up over 50% of greenhouse gasses. This is why it is the most studied and cited greenhouse gas.[16-17] However, the accumulation of these other gasses can also be attributed to the use of fossil fuel. Methane's production sources are coal, natural gas and oil. Nitrous oxide is produced from agriculture and

industrial activities and the combustion of fossil fuels, and fluorinated gasses are from a variety of industrial processes.[16] Most greenhouse gas production comes from the use of fossil fuel for energy.

The fluorinated gases constitute 3% of greenhouse gases, but they have a very high global warming potential (GWP). The production of this type of gas is not, in large part, due to the use of fossil fuel for energy. They are produced as a substitute for ozone depleting substances, electricity distribution and the manufacture of various metals and semiconductors.[18] In other words, human independence from fossil fuel for energy may have little impact in this area. Further investigations *must* be conducted as the world relies more and more on computer technology,[19] including impacts from quantum computing and A.I., to accurately predict the future of what currently stands at 3% of total greenhouse gas production.

As of 2019, approximately 97% of greenhouse gas and related 'climate change' compounds (i.e. black carbon[20]) could be reduced by human independence from fossil fuel.[21] But, *will* humans gain their independence from fossil fuel, and why do we need fossil fuel? What is it used for?

These unique hydrocarbons are found everywhere in our daily life. Their uses can be broken down into different categories including end use consumer products, industrial lubricants, energy, etc.[22] The replacement of fossil fuel in consumer products has been proven plausible by multiple innovations. Consumer product replacement only lacks cost-effective market acceptance. One logical strategy is to use renewable sources like trees, algae, crops and currently underutilized waste-streams.[23] Non-energy uses accounted for 9.3% of global use of fossil fuels, leaving 90.7% for energy production.[24]

The adoption of sustainable alternative energy is currently underway to replace fossil fuel use. As of 2019, sustainable alternatives are supplying approximately 15% of global needs. These

include nuclear power at 4.4%, hydroelectric power at 6.8% and renewables at 4.0%.[25] Supplementing *energy demand* with non-fossil fuel derived sources reduces the load on fossil fuel by 15%.

The obvious question then is; do we need fossil fuel? Short answer: yes, we *need* it. Removing fossil fuel today would destroy the entire global economy and leave billions without power, and may ultimately lead to war.[26] Long answer: no, we do not *need* it, just the energy. Humanity is putting their ingenious inventions on display every day. Advancements in energy systems are far beyond imagination, and even nuclear fusion is close.[27] But, we would still *need* to change everything to implement these new ideas and technologies. On the other hand, if there was a way to directly replace the fuel in the current infrastructure with minimal changes to said infrastructure, there would be no *need* to tap any more fossil fuel reserves for energy. And if we could make it cheap enough, the commercial world would soak it up.

So, what fits the description? Well, a lot of things. Solar power and batteries would be an expensive switch but doable. A lot of the infrastructure is already there, and according to Elon Musk, owner of Tesla Motor Company, electric power is all that is necessary. If this is the case, then sustainable renewable sources must ultimately provide the energy. Wind, hydroelectric and solar power are the strong players. However, this global conversion will take a lot of time. What can replace the liquid and gas fossil fuels right now?

Most notably; ethanol and other biofuels. Ethanol can be produced from renewable resources and is already proven to be a perfect fit for the infrastructure and consumers. In fact, it already provides 2% of the current energy demand.[28] The drawback is that it does not readily exist and must be produced through time consuming agriculture and other processes. It is currently too expensive and is subject to environmental conditions. Furthermore, this takes land, and lots of it.[28]

Another potential direct replacement is hydrogen.

An internal combustion engine can be converted to burn hydrogen for $1,000.[29] This implies that most internal combustion systems already in place can be utilized with minimal cost. Most pipes already in place for oil and natural gas can be converted to transport hydrogen by coating the pipes with compatible materials.[30-31] With the right initiative and innovation, humanity can replace fossil fuel with a clean burning fuel. 97% of all greenhouse gas production would just cease. Unfortunately, the *utopia* stops there. Most of it is currently being produced from fossil fuels, mainly through natural gas steam reformation.[32] On the *positive* side, it is not necessary to produce hydrogen from fossil fuels. Any molecule containing hydrogen is a potential source, but the byproducts must not be CO_2 or other greenhouse compounds. Hydrogen extraction from water fits this requirement. So, it can be obtained from water! *Eureka*!

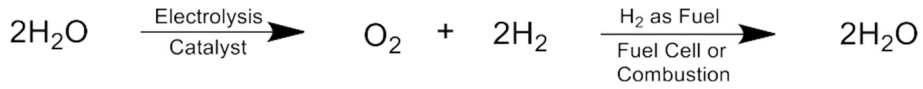

Figure 1: Typical cycle displaying the reversible and clean fuel potential of water electrolysis.

Retrieving hydrogen from water is simple in theory and proven in practice. Hydrogen gas (H_2) is a clean burning fuel with water as its combustion product (Figure 1).[33] The 'electrolysis of water' is a term that refers to the splitting of water into its constituent parts. Advancements in water electrolizers and hydrogen fuel cells that utilize this phenomenon have taken the mystery out of the chemical reaction revealing a clear map of the thermodynamics involved.[34-36] As a result, countless upgrades have been made to the efficiency of these systems. Furthermore, a new solar-to-fuel hydrogen research project, from the Israel Institute of Technology, claims efficiencies of 100%.[37] There has been a steady decrease in the production and operation costs of hydrogen-fuel-cells and water-electrolyzers.[38] Regenerative-fuel-cells are a combination of a hydrogen-fuel-cell and a water-electrolizer. The hydrogen used in advanced regenerative-fuel-cell systems[39-40] have

an energy to weight ratio, or energy density, 10 times greater than the chemicals of lithium-ion batteries.[41] This implies the future of batteries is water.

In 1970 John Bockris coined the term hydrogen fuel economy or HFE, where he spoke of replacing fossil fuels with hydrogen.[42] To see hydrogen fuel become a reality, a working HFE will need to be established. This can be done by strict government regulations or by the energy companies, including the oil industry making the switch. The current refinery locations could easily convert into hydrogen fuel production. Cost for these companies would drop even further as the land holding oil does not need to be maintained, or even purchased. This means that a working HFE would become a reality if the price of hydrogen production was low enough for it to enter the competitive market economy. The production of hydrogen from abundant water makes it an attractive choice, but hydrogen production requires the input of energy and hence cost. This cost is still too high to tip the scales in favor of the HFE. How can the cost of the energy input be addressed? Catalysts are used for a variety of tasks. Chemists use catalysts to increase the rate of a reaction and reduce the required energy input. So, the use of a catalyst will lower the cost of hydrogen production even further. The direction of the research in Dr. Jai Prakash's laboratory proceeds toward the development of these catalysts by synthetically mimicking the water splitting mechanisms found in nature.

LESSONS FROM NATURE

Synthetic production of molecular hydrogen for energy applications can be accomplished through the mimicry of the water splitting mechanisms found in photosynthesis. Photosynthesis is a very complex system of chemical reactions and processes found in organisms like cyanobacterium and the chloroplasts of plants. Within the chloroplast, there are groups of flattened sacks, known as thylakoids. This is where the light reactions of photosynthesis take place. The main components of photosynthesis involve the harvesting of light energy to transport electrons, split water into its base elements and the use of these elements in energy production and storage. In photosynthetic plants, light is absorbed by antenna pigment molecules and energizing electrons. These electrons are then passed through a series of intermediates to chlorophyll α at the reaction center. Chlorophyll α then sends the electrons down an electron transport chain where they are stored in NADPH. They are ultimately used to produce high-energy phosphate bonds through a process known as photophosphorylation. The light harvesting pigments become oxidized with less electrons. The entire process, then, cannot continue to repeat without a supply of new electrons to restore the light harvesting pigments to a reduced state. Photosynthesis extracts the fresh electrons from water.[43] This extraction of electrons from water is an oxidation process that has be traced to the membrane spanning protein called Photosystem II (PS II).[44] PS II uses the light harvesting pigments and energy from the electromagnetic radiation in the visible spectrum (~400 to 700 nm wavelengths) to both transport electrons and split water. It oxidizes and splits water using the light energy in a process called photolysis. The site of activity is an enzyme complex that catalyzes the oxidation of two H_2O molecules to molecular oxygen (O_2), four protons and four electrons. It is known as the oxygen-evolving complex or OEC. The OEC, with the help of sunlight and water, repeatedly supplies electrons for photosynthesis. These electrons are used to repeatedly reduce a

continuously oxidizing system by replacing the electrons sent down the electron transport chain.[44]

In the water splitting process the OEC, with the help of four photons, separates hydrogen and oxygen. The oxygen is expelled as molecular oxygen (O_2). The hydrogens and electrons are used to sequentially replace a missing hydrogen and electron on an adjacent tyrosine residue. The tyrosine then loses the proton and electron and the cycle repeats for each of the three remaining protons and electrons.[44] The protons are expelled into the thylakoid lumen and the electrons are used to continually reduce the system.

Elucidation of the crystal structure of PS II, at magnification of 1.9Å, revealed ~1600 water molecules scattered throughout the structure. Several of these water molecules participate in a network of hydrogen bonding, extending from the OEC to the luminal bulk phase. This hydrogen bonding network may be involved in the transport of protons from the OEC through PS II.[45] Further, the active site of the OEC has been determined to be a Mn_4CaO_5 cluster (Figure 2) held in place by an intricate protein structure including the tyrosine residue involved in proton transport.[45-46]

The OEC consists of a Mn_3CaO_4 cubane portion that includes four center-bridged oxide moieties, with the fourth Mn and oxygen positioned on the outside. The cluster is supported by six carboxylates, one imidazole and four water molecules from the surrounding protein matrix.[46] Mechanisms for O-O bond formation leading to the release of O_2 have been proposed that involve one of these adjacent water molecules.[47] There have been many attempts to reconstruct a synthetic version of the complex with similar properties, but these have met with limited success.[48-52] One of the most

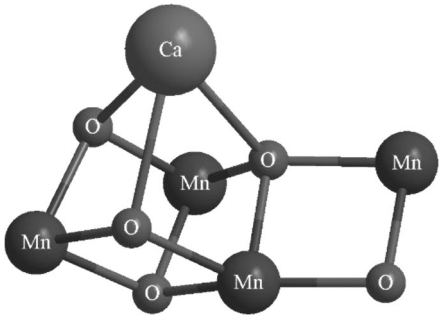

Figure 2: Proposed structure of the $CaMn_4O_5$ Cluster. (Michael Kayne created this image using Chemdraw. Adapted from Tsui, E.Y., J.S. Kanady, and T. Agapie, Synthetic cluster models of biological and heterogeneous manganese catalysts for O_2 evolution. Inorg Chem. **2013**, 52, 13833-48.)

promising methods however, used the *ligand-assisted self-assembly* procedure.[53] In this technique the final assembly of the organometallic complex is guided by specially designed ligand-structures that imitate the protein structure of PS II. These synthetic ligand backbones can be used to accurately form the desired structure and spacing of the metal ions.[51-54]

In the oxidation of water, the OEC goes through a series of oxidation (S_n) states known as the Kok Cycle (Figure 3).[45, 47] This cycle involves unique redox chemistry and is very important to understanding artificial photosynthesis.[55-56] However, synthetic systems closely mimicking the structure and function of the OEC are limited.[48-50] The *ligand-assisted self-assembly* attribute of the Mn_4CaO_5 complex[53] provides insights into the various ways it can be constructed. Ligands previously used to construct this complex include phosphinates and carboxylates.[47] These molecules had catalytic properties but not enough to provide suitable water oxidation. There have also been many ligands that use pyridine groups to chelate manganese in attempts to create water oxidation catalysts. This ligand style has been used to produce a Mn_2O_2 complex that showed oxygen evolution abilities in the presence of an oxidant. However, this is done with separate mono-nuclear ligands held together by an oxo-bridge.[57] Multi-nuclear ligands have been produce that incorporate calcium into a Mn_3CaO_4 cluster. These complexes showed that trinucleating ligands are possible, and further displayed that Ca^{2+} was necessary for the complex to reach higher oxidation states.[48]

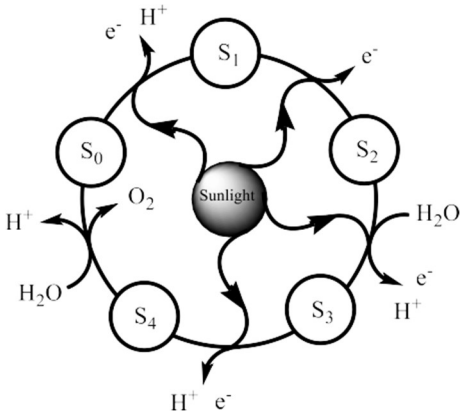

Figure 3: Visual representation of the KOK cycle showing water oxidation and intermediate steps. (Michael Kayne created this image using Chemdraw. Adapted from Tsui, E.Y., J.S. Kanady, and T. Agapie, Synthetic cluster models of biological and heterogeneous manganese catalysts for O_2 evolution. Inorg Chem. **2013**, 52, 13833-48.)

Synthetic reproductions that attempt to exactly mimic the native protein structure of the OEC have been produced. These come very close to the structure and functionality of the native

complex, but the inability to control competing ligands prevents their interaction with surrounding water molecules and the complete oxidation changes of certain manganese atoms.[49] A successful synthetic OEC needs to incorporate 4 manganese into a complete cubane and dangler style core to lower the barrier to O-O bond formation.[47] However, attempts at correctly synthesizing the proper cluster geometry have resulted in limited coordination flexibility around the manganese atoms. The flexibility of the coordination chemistry is necessary to provide the activation of two water molecules.[50]

To combat these challenges, it is proposed that the best course of action, in the synthesis of a water oxidation catalyst closely mimicking the OEC, is through stand-alone multi-nuclear ligands. This can be accomplished by using cyclic organic compounds such as triazacyclononane and tetraazacyclotetradecane. These molecules have been previously used in various types of coordination chemistry.[58-59] However, it is intended that these molecules serve as a backbone using linker chains to metal-binding units based on N- and O- atom donor functionality such as polypyridines, amines and carboxylates (Figure 4). The choice of unit will favor previously published systems that have shown an ability to form stable, high-valent, Mn-oxygen intermediates.[48] Macrocyclic multinuclear metal complexes like these have been produced with a variety of backbone styles, metals and intended substrates.[60]

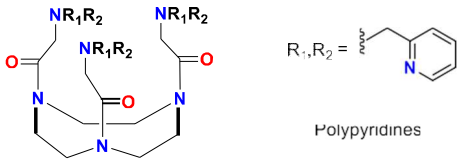

Figure 4: Cyclam-based macrocycle with linkers and the choice of polypyridines as metal binding units.

The versatile nature of this style of ligand provides a vast array of pathways for the assembly of the tetra-manganese complex. Ligands with multiple metal binding sites (coordination centers) have been made that closely resemble the structural stability of the OEC[48]. They provide proof that a structural backbone, capable of hosting multiple binding sites is possible. These

backbone and linker style structures provide a means for testing the properties and effects of a variety of molecules capable of participating in metal-binding.

REACTION THERMODYNAMICS

The photochemical reaction involving the splitting of water inherent in plants and some single cell organisms is generally as follows:

$$H_2O + Energy \rightarrow 2H^+ + 2e^- + \frac{1}{2}O_2 \qquad (1)$$

The protons separated from water are used to create a gradient activating biomechanical machinery such as ATP synthase, producing adenosine triphosphate (ATP). These molecules are then used as energy. Similarly, water split synthetically yields protons, electrons and oxygen that can be used for a large variety of applications. One application being the desired clean energy production. There are also end uses by these organisms in nature from which we can learn a lot. However, in this thesis, it is not how organisms *use* the products obtained from H_2O that is of interest, but how organisms catalyze the separation. This involves the oxygen evolving complex (OEC) of photosystem II.

The electrochemical splitting of water into its constituent parts is not thermodynamically favorable at standard temperature and pressure. To understand why, the general equation can be separated into half reactions and examined in relation to Gibbs free energy.

These standard reduction potentials, or half reactions, are examined in electrochemistry through the analysis of the activity at the anode and cathode denoting either oxidation or reduction respectively. The oxidation reaction (anode) portion of water oxidation has a standard potential of 1.23 V compared to a normal hydrogen electrode at standard temperature and pressure (STP).[61]

$$2H_2O \rightarrow 4H^+ + 4e^- + O_2 \qquad E^\circ = +1.23\ V \qquad (2)$$

This is followed by the reduction reaction (cathode) portion which has a standard potential of 0.00 V and is noted as:

$$4H^+ + 4e^- \rightarrow 2H_2 \qquad E^\circ = +0.00\ V \tag{3}$$

And

$$E^\circ_{rxn} = E^\circ_{red} - E^\circ_{ox} \tag{4}$$

$$-1.23\ V = 0.00\ V - 1.23\ V \tag{5}$$

Gibb's free energy, considering the 4 electrons required to produce a single O_2 molecule from two water molecules is:

$$\Delta G^\circ_{cell} = -nFE^\circ_{cell} \tag{6}$$

$$475\frac{kJ}{mol} = (-4\frac{e^-}{mol})\,(96.485\frac{kJ}{V})\,(-1.23V) \tag{7}$$

Water oxidation to H_2 and O_2 is nonspontaneous and requires the input energy of at least 475 kJ/mol1.23 V. *E* is related to the electromagnetic spectrum through this equation:

$$h\nu = \frac{hc}{\lambda} \tag{8}$$

Where *hv* is photon energy (*hv = E; eV*), h is the Plank constant ($4.14*10^{-15}$ eV/s), c is the speed of light (in a vacuum: $3.00*10^8$ m/s) and λ is the wavelength of the photon energy. This equation tells us that Sunlight, including all the visible spectrum and some of the infrared spectrum, can be used as the energy source and is shown by utilizing the rearranged *hv* equation:

$$\lambda = \frac{hc}{h\nu} \tag{9}$$

$$\lambda = \frac{(4.14 * 10^{-15} eV * s) * (3.00 * 10^8 \frac{m}{s})}{1.23eV} \tag{10}$$

$$\lambda = 0.00000101\ m = 1010\ nm \tag{11}$$

All wavelengths shorter than approximately 1000 nm theoretically have enough energy to electrolyze water. This however is in ideal conditions and does not account for the increase in needed energy from the associated overpotential.[62] Overpotential (OP), in this case, increases the

1.23 eV thermodynamically required due to a variety of circumstances involving efficiencies (i.e. cell design, resistance, current density, electrode material, bubble formation, concentration, pH, deviation from STP, etc.).

ΔG with the addition of OP effects must be considered to accurately calculate the required energy and analyze the effect of a catalyst.

THE THESIS

The assembly of the Mn_4CaO_5 cluster has been envisioned following two different approaches. Each approach also utilizes iron (II) metal centers along with manganese (II) to compare the redox capabilities of each metal. The first approach requires synthesis of a ligand containing four metal-binding units to accommodate the four M atoms (M = Mn^{2+} or Fe^{2+}) present in the cluster. The M_4L complex (L = synthetic ligand) may then be oxidized in the presence of Ca^{2+} to directly yield the M_4CaO_5 cluster. Similar strategies have been used to produce a Mn_3CaO_4 core from a Mn_3L complex.[48] The second approach involves the synthesis of a ligand with only three metal-binding sites to first construct a M_3CaO_4 cubane core.[48] This is then oxidized in the presence of Ca^{2+} with either a high-valent metal-oxygen species, or a separately synthesized single metal-binding ligand (mononuclear) M-complex, to produce the desired Mn_4CaO_5 cluster. The goal of producing a complex catalyst that can mimic the Mn_4CaO_5 cluster is completed in part in this thesis and will be continued by graduate students in Dr. Jai Prakash's Laboratory at Texas A&M University Corpus Christi.

Four organometallic complexes are synthetically produced to mimic the actions of the OEC of PS II. They are characterized using various spectroscopic techniques. This includes a three-metal-binding and a four-metal-binding ligand. Each ligand is complexed separately with Mn^{2+} and Fe^{2+}. The iron complexes are built alongside the manganese complexes to evaluate whether the cheaper and more easily obtainable iron metal is a rational replacement for the relatively less abundant and more expensive manganese metal. In future work the synthetic complexes will be oxidized in the presence of Ca^{2+} (to form the M_4CaO_5 complex) and evaluated for catalytic efficiency, redox potential and their ability to produce protons and electrons for use in energy applications.

RESULTS AND DISCUSSION

Synthesis of The Ligands. Our studies commenced with the syntheses of chelating ligands designed to host multiple coordination centers capable of binding three and four metal ions concurrently within the same ligand framework (Figure 5). These are 1,1',1''-(1,4,7-triazonane-1,4,7-triyl)tris(2-(bis(pyridin-2-ylmethyl)amino)ethan-1-one) or TACNAcDPA on the left and 1,1',1'',1'''-(1,4,8,11-tetraazacyclotetradecane-1,4,8,11-tetrayl)tetrakis(2-(bis(pyridin-2-ylmethyl)amino)ethan-1-one) or CyclamAcDPA on the right.

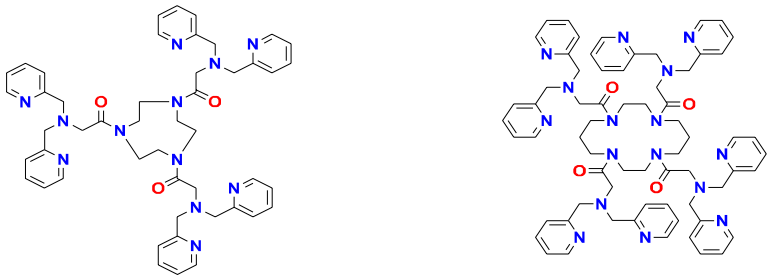

Figure 6: Structure of the ligands synthesized in this work. TACNAcDPA (left) and CyclamAcDPA (right) are designed to bind with three and four metal ions,

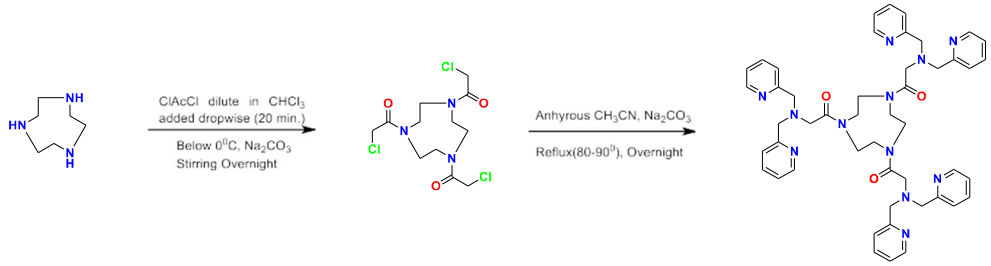

Figure 5: Synthetic scheme to produce TACNAcDPA ligand.

Synthesis of TACNAcDPA Ligand. The synthesis of TACNAcDPA was achieved in two steps following the synthetic scheme shown in Figure 6.

The synthesis of TACNAcCl (Scheme 1) was performed at subzero Celsius temperature to minimize unwanted S_N2 reactions at the α-carbon of the chloroacetyl chloride (i.e., substitution of the -Cl group at the α-carbon in chloroacetyl chloride by one of the N atoms of the TACN). The preferred reaction is the nucleophilic acyl substitution reaction where a relatively more reactive acyl-Cl atom is substituted by one of the N atoms of the TACN to give an amide bond. This was done using an ice bath with NaCl salt

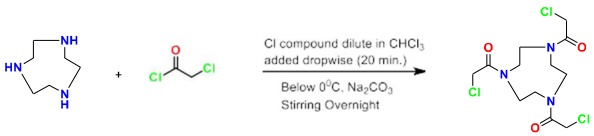

Scheme 1: Synthesis of 1,1',1''-(1,4,7-triazonane-1,4,7-triyl)tris(2-chloroethan-1-one)

added to reduce the temperature of the reaction (Figure 7). As an extra precaution against side reactions, the chloroacetyl chloride was diluted in the chosen reaction solvent, i.e., chloroform ($CHCl_3$) and added dropwise to the main reaction flask containing TACN $CHCl_3$ solution over 20 to 30 minutes. The reaction was carried out in the presence of sodium carbonate (Na_2CO_3) dissolved in water as a base, and the reaction flask was wrapped in aluminum foil to prevent light exposure. This is due to chloroacetyl chloride's susceptibility to undergo hydrolysis reaction in the presence of light.

Figure 7: Reaction setup in the synthesis of TACNAcCl..

This reaction was left overnight, and the next day, the reaction mixture was extracted with deionized water (DI-H_2O), keeping the organic layer. Previous attempts to produce this compound were done using triethylamine (Et_3N) as a base, which resulted in a successful reaction. However, the use of Et_3N is undesirable due to the difficulty in the liquid-liquid extraction step of the work up. A large quantity of black solid material adheres heavily to the separatory funnel and proves to be difficult to remove. The black solid traps a portion of the desired product and causes a reduction in yield. Na_2CO_3 dissolved in water, as a base, proved to be the easier route and had the added benefit of producing a white solid product and higher yield.

The organic layer was cleaned using DI-H_2O and dried over Na_2SO_4 to give the desired compound as a solid precipitate. This was done by evaporating the $CHCl_3$ (the reaction solvent) to approximately 75 mL (if all the solvent is evaporated, the solid is difficult to dissolve again). It was then diluted slowly with a nonpolar solvent. Both hexane and diethyl ether have identical behavior when diluting from both $CHCl_3$ and DCM allowing for some flexibility in the choice of dissolving and diluting solvents during workup.

A white powder precipitated during the dilution process and could be filtered from the solvent using a fritted filter. The filtrate was evaporated to 25 mL and diluted again with nonpolar solvent to yield more product. The filter cake showed near purity based on its ^{1}H-NMR spectrum. However, higher purity can be obtained by column chromatography using basic alumina as a stationary phase. The mobile phase included hexane as the starting solvent. The polarity was then rapidly increased to 100% ethyl acetate (EtOAc). The 100% EtOAc eluted most of the impurities verified with thin layer chromatography (TLC) tests. The high-purity product finally elutes when the polarity of the mobile phase is increased using methanol (MeOH) to a ratio of no more than 95:5:EtOAc:MeOH, leaving the rest of the impurities trapped in the column.

Purification using column chromatography is not necessary for the next reaction when Na_2CO_3 is used as a base. Both the post and precolumn products were used in separate runs of Scheme 2 with near identical yields. This means that the product loss due to column purification is not necessary for the purpose of building the final ligand; TACNAcDPA.

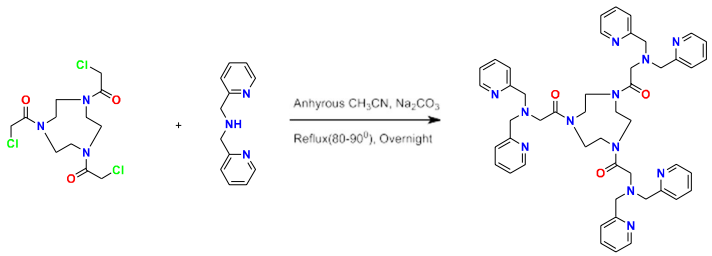

Scheme 2: Synthesis of 1,1',1''-(1,4,7-triazonane-1,4,7-triyl)tris(2-(bis(pyridin-2-ylmethyl)amino)ethan-1-one).

TACNAcCl undergoes an S_N2 nucleophilic aliphatic substitution reaction that requires elevated temperatures in order to initiate substitution of the chlorine atom in the alkylhalide bond with the reactant dipicolylamine (DPA). Acetonitrile (CH_3CN) has a relatively high boiling point (~82 ºC) making it a good, high temperature solvent. TACNAcCl, has a very low solubility in both $CHCl_3$ and DCM, but it has a high solubility in CH_3CN. Therefore, scheme 2 utilizes CH_3CN as the reaction solvent. Additional anhydrous conditions are also necessary to avoid cleavage of the amide bonds in TACNAcCl.

TACNAcCl was reacted with DPA in the presence of Na_2CO_3 as a base. This reaction mixture was refluxed in CH_3CN at ~90 ºC, using an oil bath (Figure 8). The reflux condenser was capped with nitrogen flow to avoid the introduction of air and moisture to the reaction and to provide an outlet for pressure fluctuations. The stirring was set at full speed to keep the Na_2CO_3 suspended in the reaction mixture and it was left to reflux overnight. In other attempts to synthesis this compound, the reaction was left running for several days with no change to the final yield.

Figure 8: Reflux condenser setup of DPA addition reaction.

After 24 hours, the reaction mixture was cooled and filtered to remove the solid unreacted Na_2CO_3, leaving a dark but clear yellowish orange colored filtrate. All the CH_3CN in this solution was evaporated resulting in a viscous, sticky, orange substance. It readily dissolved in DCM and was washed with acidic DI-H_2O. Neutral water extraction, results in a small loss of the product, while acidifying the water prevents this loss. Evaporation of the dried solvent revealed a dark, caramel-red, sticky, highly viscous substance.

A small amount of easily removed impurities remained. These were eliminated by dissolving the compound in EtOAc and filtering several times. This was done until no more precipitate was observed. The remaining unreacted DPA prevents the formation of solid product. The substance was dissolved it in a tiny amount of DCM, and then diluted very slowly with hexane. The solution became cloudy, forming a sticky, solid, reddish precipitate.

The compound was dissolved and evaporated several times using DCM to remove any trapped hexane and EtOAc solvents. This compound exhibited a very dark red color and was far

Figure 9: Column chromatography showing separation of unreacted DPA.

more viscous but not solid. ^{1}H-NMR showed this substance still had a small amount of unreacted DPA that was trapped tightly within the desired compound. The yield of this crude product was close to 97%, but the unreacted DPA must be completely removed before the compound could be complexed with metal to avoid solo DPA complex formation.

Further purification was accomplished by column chromatography equipped with basic alumina as the stationary phase. The mobile phase included hexane as the starting solvent and switching to 100% EtOAc until all DPA was removed (Figure 9). Once all the DPA had eluted, the polarity of the mobile phase was increased using MeOH up to a maximum of 95:5:EtOAc:MeOH. The desired eluent was then evaporated and dissolved in DCM several times to remove the mobile phase solvents. After evaporating all the remaining solvent a popped rice-like substance (Figure 10) remained that is very bright neon, orangish-pink in color. Performing column chromatography on the compound was an efficient way to obtain the purified ligand (TACNAcDPA) to be used in metalation reactions with a purified yield of over 85%.

Figure 10: Final ligand displaying the pink color associated with purity.

Synthesis of CyclamAcDPA Ligand. The synthesis of CyclamAcDPA was achieved in two steps following the synthetic scheme shown in (Figure 11).

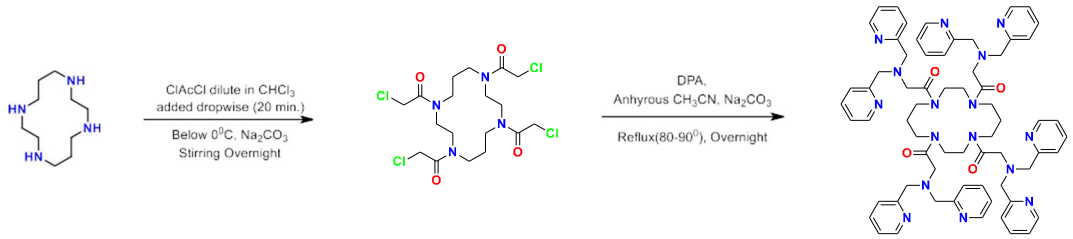

Figure 11:Synthetic scheme to produce CyclamAcDPA ligand.

The CyclamAcDPA ligand made use of a four nitrogen azamacrocyclic moiety as the base platform known as tetraazacyclotetradecane (cyclam). ChloroAcetyl chloride was added to the cyclam structure at the nitrogen atoms using a similar nucleophilic acyl substitution reaction to scheme 1 (Scheme 3) to produce CyclamAcCl. Differences in the two reactions become apparent during workup. A foamy layer was found floating on top of the completed reaction mixture. This foamy layer dissolved in a small amount of water and was added to the water from the reaction. Most of the desired compound was found in the organic (CH_3CN) layer, however some compound was extracted from the aqueous layer using DCM.

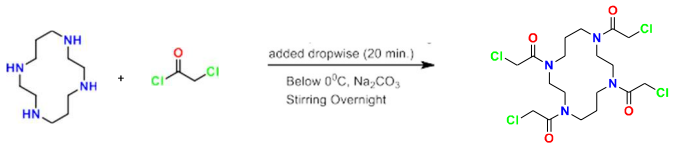

Scheme 3: Synthesis of 1,1',1",1'"-(1,4,8,11-tetraazacyclotetradecane-1,4,8,11-tetrayl)tetrakis(2-chloroethan-1-one).

The organic solvent containing the compound was evaporated to about 75 mL. It was then diluted with hexane and a faintly yellowish, white gel precipitated. Unlike the TACNAcCl product this gel dissolved readily in DCM. It showed near purity, based on ^{1}H-NMR characterization. Further purity was obtained by column chromatography using basic alumina as the stationary phase. The mobile phase included hexane as the starting solvent. EtOAc was used to slowly increasing the eluent polarity followed by MeOH. The final eluent ratio was no more than

90:10:EtOAc:MeOH. The substance bubbled up to a solid on vacuum producing a white, sticky, popped rice-like compound (Figure 12).

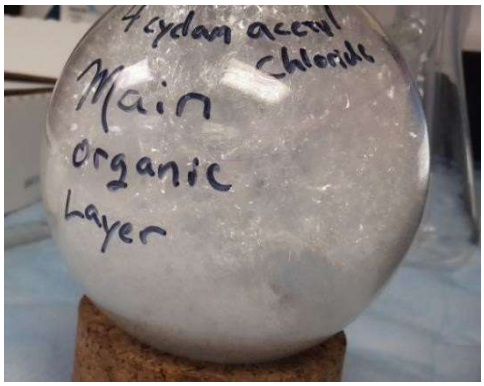

Figure 12: Final reaction product, CyclamAcCl, after purification using column chromatography.

The product CyclamAcCl was used in the synthesis of CyclamAcDPA. This reaction also followed the same reflux reaction set up and a similiar S_N2 reaction as Scheme 2 (Scheme 4). The reaction solution was filtered, washed with DI-H_2O and evaporated completely revealing a dark amber-colored, sticky gel (Figure 13).

Production of a gel (instead of solid) is due to the presence of unreacted DPA. The DPA was removed with a nonpolar solvent (i.e. hexane, Et_2O). It was then purified further by dissolution of the substance in EtOAc causing a dark precipitate that was filtered using cotton and evaporated several times until no solids precipitated. This step was done very slowly to avoid the entrapment of the desired compound within the precipitate impurity. The impurity had no ^{1}H-NMR visibility, but it did contribute to the brownness of the compound. The EtOAc soluble compound was evaporated and a less brown, dark-red compound with limited popped rice-like structure remained. Column chromatography was used to remove trace impurities and the small amount of unreacted DPA that prevented the compound from exhibiting a fully popped rice-like solid with an orangish-red color.

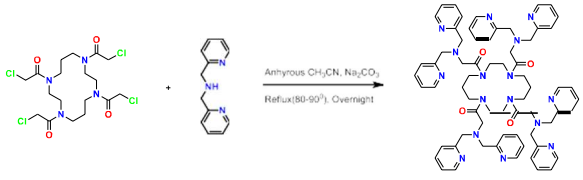

Scheme 4: Synthesis of 1,1',1",1'"-(1,4,8,11-tetraazacyclotetradecane-1,4,8,11-tetrayl)tetrakis(2-(bis(pyridin-2-ylmethyl)amino)ethan-1-one).

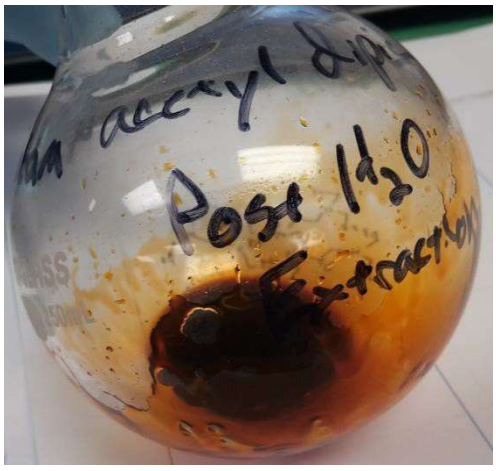

Figure 13: Dark orange/red color of the post-reaction substance (CyclamAcDPA).

All the organic compounds were thoroughly characterized using ^{1}H-NMR, ^{13}C-NMR, and FT-IR. Moreover, the compounds CyclamAcCl and CyclamAcDPA were also characterized by mass spectrometry.

Synthesis of The Metal-Ligand Complexes. Metalation reactions with the synthesized ligands were done using iron(II) triflate and manganese(II) triflate salts. Fe(II)/Mn(II)$(OTf)_2$ (OTf^- = triflate ion, $CF_3SO_3^-$) were selected as the metal precursors because the triflate ion, being a weak coordinating anion, can easily be displaced from the metal center in the complex by solvent molecules such as acetonitrile or water, providing a labile active site at the metal center that is crucial for catalysis. The presence of chloride ions, from the Fe(II)/Mn(II)Cl_2 precursor, are avoided in the metal complexation process because they are hard to displace from the metal centers.

Synthesis of Metal Triflates. To prepare the Mn(II)$(OTf)_2$, $MnCl_2$ was reacted with trimethylsilyl trifluoromethanesulfonate (TMSOTf) in CH_3CN solvent. It is important to perform this preparation in a nitrogen (N_2) atmosphere due the reactivity in oxygen and moisture of both the metal chloride and TMSOTf.

The mixed solution was a turbid slurry that was warm to the touch. After a few minutes the solution homogenized into a clear pink color. Next day, the solution had a clear yellowish-pink color. The solution was filtered using a syringe filter and evaporated revealing a powder. This powder was dissolved in CH_3CN, layered with Et_2O (Figure 14) and placed in the glovebox freezer. After 24 hours, a slightly pink, white

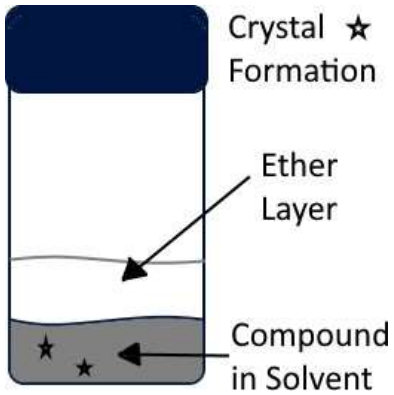

Figure 14: Setup of crystallization by solvent layer diffusion.

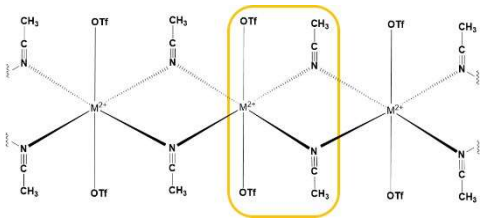

Figure 15: General crystal structure of $M(OTf)_2(CH_3CN)_2$ where M is the transition metal.

precipitate powder with the formula $Mn(OTf)_2(CH_3CN)_2$ (Figure 15) was obtained by decanting the container, washing the precipitate with Et_2O, and drying the powder on high vacuum. The previously decanted solvent was evaporated to 5 mL and the Et_2O layering was repeated to yield the remaining unprecipitated metal triflate.

$Fe(OTf)_2(CH_3CN)_2$ was obtained in the same way using $FeCl_2$. The differences include the initial cloudy slurry changed to a clear purple after a few minutes, after 24 hours it appeared as a clear yellowish-purple solution and the final dry product was a faint green white powder.

Synthesis of $Mn(II)_3(L)(OTf)_6 \bullet xCH_3CN$ (L = TACNAcDPA). The metalation reaction was carried out in a nitrogen atmosphere to ensure minimal oxygen/moisture exposure. The TACNAcDPA ligand was reacted with 3.2 equiv. prepared manganese triflate salt in CH_3CN solvent (Scheme 5). The brownish orange solution was left stirring overnight. (This reaction was attempted using DCM with very limited success due to the metal triflate's insolubility in DCM). After 24 hours, the solution was filtered using a syringe filter and evaporated to 5 mL. This remaining solvent contained the desired compound and was used to crystallize the compound by very carefully layering the solution with diethyl ether (Et_2O) as to not mix the layers allowing for slow diffusion mixing over time (Figure 14). To obtain higher purity, the diffusion could be slowed down by placing the container in the freezer over several days. This produced a white/brownish-orange solid. This was further dissolved in CH_3CN, filtered and layered with Et_2O for a second

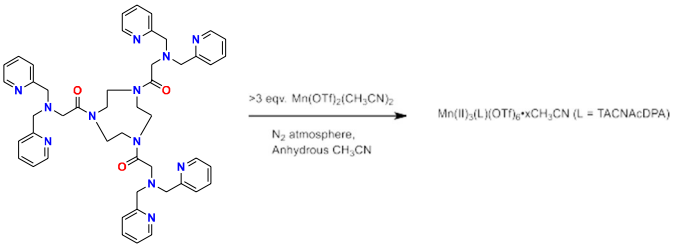

Scheme 5: Synthesis of Mn (II) complex of 1,1',1''-(1,4,7-triazonane-1,4,7-triyl)tris(2-(bis(pyridin-2-ylmethyl)amino)ethan-1-one).

crystallization and slightly higher purity with just over 70% yield.

Synthesis of $Fe(II)_3(L)(OTf)_6 \bullet xCH_3CN$ (L = TACNAcDPA). The metalation reaction using iron triflate was performed similar to Scheme 5 (Scheme 6). The initial color of the mixture, however, was a dark brown that turned to a dark green overnight. The crystallization product was a dirty white solid with a brownish-green tint. This reaction can be done in either CH_3CN or DCM with yields reaching almost 90%.

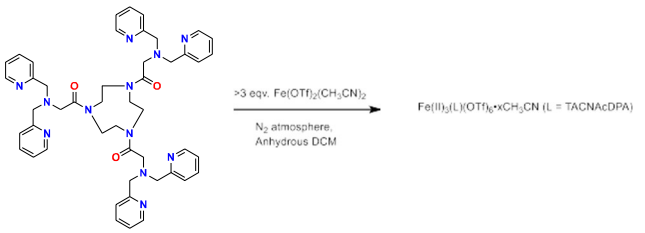

Scheme 6: Synthesis of Fe(II) complex of 1,1',1''-(1,4,7-triazonane-1,4,7-triyl)tris(2-(bis(pyridin-2-ylmethyl)amino)ethan-1-one).

Synthesis of $Mn(II)_4(L)(OTf)_8 \bullet xCH_3CN$ (L = CyclamAcDPA). The CyclamAcDPA ligand was reacted with 4.2 equiv. prepared manganese triflate (Scheme 7 & Scheme 8 respectively) in a N_2 atmosphere to avoid the introduction of O_2 and moisture to the reaction.

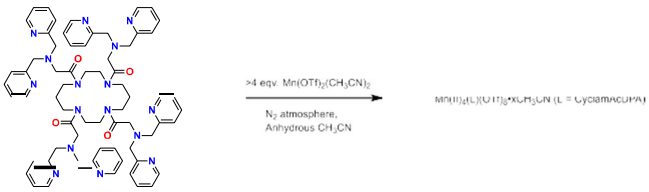

Scheme 7: Synthesis of Mn (II) complex of 1,1',1'',1'''-(1,4,8,11-tetraazacyclotetradecane-1,4,8,11-tetrayl)tetrakis(2-(bis(pyridin-2-ylmethyl)amino)ethan-1-one).

This reaction was first performed using DCM as a solvent. This was met with limited success. ^{1}H-NMR of the metal complex only showed resonances in 1 – 10 ppm range. So, the reaction was performed in CH_3CN. It began as a clear dark orange color, and 24 hours later the solution had no change in color. (When the same reaction was done in DCM there was change in color from dark

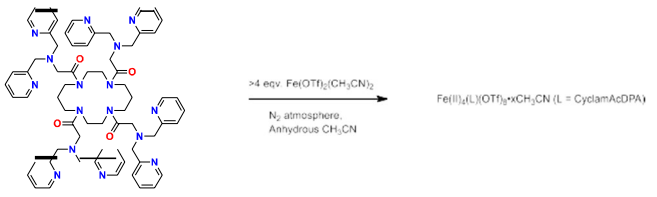

Scheme 8: Synthesis of Fe (II) complex of 1,1',1'',1'''-(1,4,8,11-tetraazacyclotetradecane-1,4,8,11-tetrayl)tetrakis(2-(bis(pyridin-2-ylmethyl)amino)ethan-1-one).

orange to a neon orange moments after manganese triflate addition and after 24 hours it had separated into two semi-cloudy layers.)

The reaction mixture was filtered using a syringe filter and evaporated to ~5 mL. This solution was carefully layered with Et_2O to avoid mixing and placed in the freezer for several days for crystallization. A white/faint-pink solid remained caked to the bottom of the container. The liquid was decanted, and the solid was dried and CH_3CN was added to the vial. This pulled the pink color of the solid but did not dissolve the solid. This solvent was immediately decanted. CH_3CN was again added to the solid, and it took just over just over a minute to dissolve. The solution was layered with Et_2O, capped and returned to the freezer for crystallization. After several days, the liquid was decanted to find a pinkish white crystal layer which was just over a 60% yield.

The problems with this reaction could be related to a spike in O_2 levels (within the glovebox) that occurred during the final steps of the reaction.

Synthesis of $Fe(II)_4(L)(OTf)_8 \bullet xCH_3CN$ (L = CyclamAcDPA). The reaction of CyclamAcDPA and iron triflate with CH_3CN as a solvent (Scheme 8) started as a cloudy brown solution and begun to gain a darker brown color after few minutes. Next day, the solution had turned green. This solution was filtered and evaporated to approximately 5 mL. It was then prepared for crystallization by carefully layering it with Et_2O and placing it in the freezer. However, an alternate crystallization method was used. The scintillation vial containing the compound solution was evaporated to 5 mL and placed into a larger crystallization chamber with Et_2O (Figure 16). This provided an extremely slow diffusion of Et_2O into the compound solvent (7+ days). The

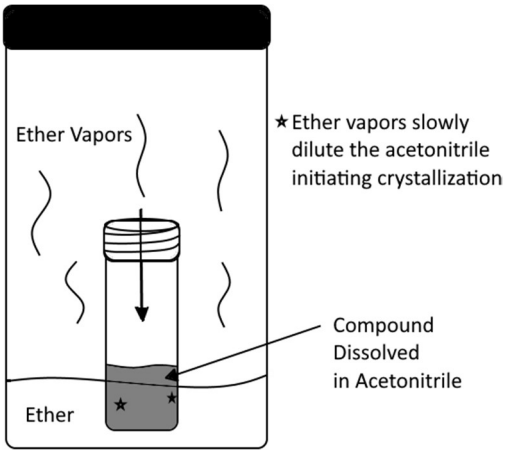

Figure 16: Typical setup of crystallization chamber.

crystallization product was a white to dirty green solid at almost an 80% yield.

The terminal DPA structure of each metal complex will theoretically have the coordination chemistry of other similar Mn^{2+} and Fe^{2+} mononuclear chelation sites that utilized the DPA structure reported in the literature (Figure 17). It is also possible that the metal ion is bonded to other parts of the center structure such as the oxygen bonded to the first carbon from the central ring. However, the exact structure cannot be elucidated until further data is collected i.e. mass and crystallographic data.

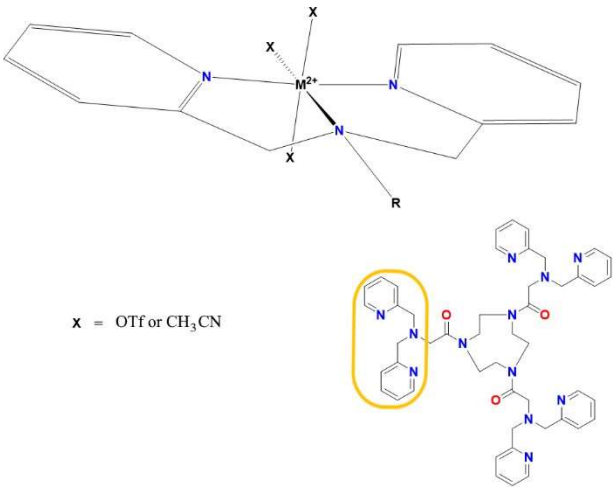

Figure 17: Proposed coordination of the terminal DPA to the metal center where X = CH_3CN or OTf.

Characterization of Metal-Ligand Complexes. To elucidate the structure of metal-ligand complexes, they were analyzed by ^{1}H-NMR, UV-Vis and FT-IR. Several attempts were made to grow single crystals of these metal complexes suitable for X-ray diffraction, but only crystalline powder was obtained. The evidence of metal sites in these complexes came from the ^{1}H-NMR studies. The resonances in the ^{1}H-NMR of all metal complexes fell out of traditionally observed chemical shift values of 0 ppm to 10 ppm for diamagnetic molecules. For example, the resonances in the ^{1}H-NMR of the iron complex of CyclamAcDPA fall between 150 ppm to -50 ppm (Figure 18; Data Set 2.4.1 in appendix). This result illustrates that this complex is paramagnetic in nature, and high-spin Fe(II) centers are present in

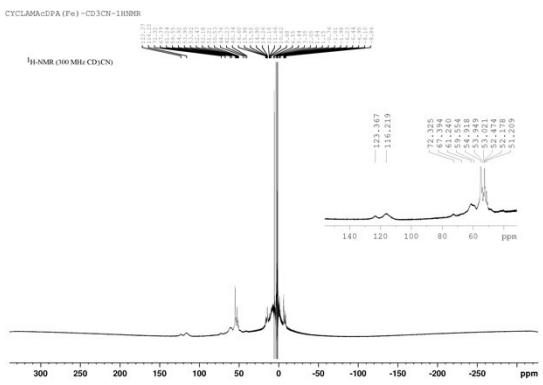

Figure 18: ^{1}H-NMR of $Fe(II)_4(L)(OTf)_8$•xCH_3CN (L = CyclamAcDPA).

this complex. Similar inferences can be concluded from the ^{1}H-NMR of all other metal complexes. The UV-Vis absorption spectrum of these complexes does not display any major absorption peak in the visible region (Figure 19; Data Set 2.3.2 & 2.4.2 in appendix). This is common for Fe(II)- and Mn(II)-complexes. Most of these complexes are not brightly colored to provide any strong absorption peak in the visible region. The FT-IR spectrum of these metal complexes exhibits a peak at ~ 1600 cm^{-1} corresponding to the carbonyl stretch from the ligand framework. Studies are underway to determine the number of metal centers in these complexes along with the number of solvent molecules i.e., CH_3CN, if any. The CH_3CN molecule usually binds to metal centers in the metal complexes if a weak coordinating counterion such as triflate is present.

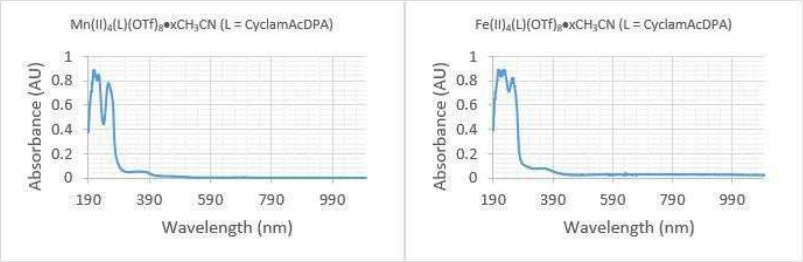

Figure 19: UV-Vis absorption spectrum of $Mn(II)_4(L)(OTf)_8$ (Left), $Fe(II)_4(L)(OTf)_8$ (Right), L = CyclamAcDPA.

CONCLUSION AND FUTURE DIRECTIONS

Iron- and manganese-based multinuclear transitional-metal complexes supported by rationally designed ligands, aimed at mimicking the function of biological water oxidation site in photosystem II (i.e. the OEC) have been produced and a clear synthetic pathway has been established. The supporting ligands were designed in such a way that they can accommodate three or more metal centers within the same ligand framework. This aspect of ligand design is important because the multi-metallic core makes it easier to follow the chemical and structural changes occurring at the metal centers during any chemical transformation. In order to achieve that, we synthetically incorporated multiple (mainly three and four) metal-binding units in the same ligand framework using azamacrocyclic compounds (tacn and cylcam) as the basal platform. The multiple binding units ensure the formation of trinuclear and tetranuclear metal clusters. This synthesis was successfully achieved in two steps starting with commercially available materials. All the reaction steps were high yielding (75 – 86 %). The final ligands, TACNAcDPA and CyclamAcDPA, were further purified by column chromatography, given the complexity of these ligands as they contain multiple N atoms (>12), making their purification difficult. The purification was achieved by gravity chromatography rather than flash chromatography as both product and impurity had similar retention factors on the column. All organic compounds were fully characterized by ^{1}H-NMR, ^{13}C-NMR, and IR. CyclamAcCl and CyclamAcDPA were also characterized by mass spectrometry. The metal complexation with TACNAcDPA and CyclamAcDPA ligands were successfully achieved inside an inert gas glovebox to produce corresponding iron- and manganese-ligand complexes. Several attempts were made to grow single crystals of these metal complexes so that their structure can be determined but these complexes couldn't be recrystallized. The ^{1}H-NMR of these complexes displayed resonances between 150 ppm to -50 ppm suggesting that these

complexes are paramagnetic in nature. This also indicated that the metal complexation with the ligands were successful and these complexes contain metal sites making them paramagnetic. The UV-vis absorption spectrum of these complexes did not show any absorption band in the visible region. However, the FT-IR spectrum of all these complexes showed a peak at ~1600 cm^{-1}, corresponding to the carbonyl group from the ligand framework. Further analysis to completely characterize these metal complexes are underway. The TACNAcDPA ligand is expected to produce trinuclear metal clusters with a general formula $M(II)_3(L)(OTf)_6 \bullet xCH_3CN$ (M = Fe and Mn; L = TACNAcDPA; x = an integer number) whereas the CyclamACDPA ligand is expected to produce tetranuclear metal clusters with a general formula $M(II)_4(L)(OTf)_8 \bullet xCH_3CN$ (M = Fe and Mn; L = TACNAcDPA; x = an integer number).

Future studies include determining the efficiency with which these metal complexes oxidize water electrochemically to produce H_2 gas. These complexes will further be subjected to chemical oxidation using H_2O_2 or PhIO to generate high-valent metal-oxygen species to study the mechanism of water oxidation. This mechanistic study will help us design efficient and practical water oxidation catalysts, providing the world with a cheap and clean energy, H_2.

REFERENCES

1. McLamb, E. The Secret World of Energy. https://www.ecology.com/2010/09/15/secret-world-energy/ (accessed 20 January 2020).
2. Libavius, A., *Alchemica*. 1597.
3. Hsu, C. S.; Robinson, P. R., Petroleum Distillation. In *Springer Handbook of Petroleum Technology*, Springer: 2017; pp 533-550.
4. Neumann, C.; Lewis, W., *The Chemical Works of Caspar Neumann*. J. and F. Rivington: 1773; Vol. 2.
5. Landes, D. S., *The unbound Prometheus: technological change and industrial development in Western Europe from 1750 to the present*. Cambridge University Press: 2003.
6. John Alkin, B. E. H., To the Editor of the Monthly Magazine. *The Monthly Magazine* **1798,** *4*.
7. Hall, G.; Newell, S., *The Conversion of the World: Or, The Claims of Six Hundred Millions and the Ability and Duty of the Churches Respecting Them*. American Board of Commissioners for Foreign Missions: 1818.
8. Coxe, J. R., *Consideration Respecting the Recognition of Frinds in Another World...* George S. Appleton: Philadelphia, 1845.
9. Robinson, B., Victorian Medicine—From Fluke to Theory. *BBC History. British History in depth: Victorian Medicine* **2010**.
10. Coren, M. J. The Speed of Europe's 18th-century Sailing Ships is Revamping History's View of the Industrial Revolution. (accessed 30 December 2019).
11. Modak, J. M., Haber process for ammonia synthesis. *Resonance* **2002,** *7*.
12. Raudzens, G., War-winning weapons: the measurement of technological determinism in military history. *The Journal of Military History* **1990,** *54*, 403.
13. Hartcup, G., *The war of invention: scientific developments, 1914-1918*. Potomac Books Incorporated: 1988.
14. Smil, V., Detonator of the population explosion. *Nature* **1999,** *400*, 415-415.
15. Skuce, A. Critical Angle: Reflections on the Refractory Problems of Climate and Energy. https://critical-angle.net/2015/04/01/emissions-history-and-the-great-acceleration/ (accessed 31 December 2019).
16. Contributors, E. Overview of Greenhouse Gases. https://www.epa.gov/ghgemissions/overview-greenhouse-gases (accessed 31 December 2019).
17. James H. Butler, S. A. M. The NOAA Annual Greenhouse Gas Index (AGGI). https://www.esrl.noaa.gov/gmd/aggi/aggi.html (accessed 31 December 2019).
18. Contributors, E. Emissions of Fluorinated Gases. https://www.epa.gov/ghgemissions/overview-greenhouse-gases#f-gases (accessed 31 December 2019).
19. Gottschalk, S., *The terminal self: Everyday life in hypermodern times*. Routledge: 2018.
20. Contributors, E. Black Carbon. https://www3.epa.gov/airquality/blackcarbon/ (accessed 31 December 2019).
21. Lelieveld, J.; Klingmüller, K.; Pozzer, A.; Burnett, R. T.; Haines, A.; Ramanathan, V., Effects of fossil fuel and total anthropogenic emission removal on public health and climate. *Proceedings of the National Academy of Sciences* **2019,** *116*, 7192-7197.
22. Contributors, I. Importance of Fossil Fuels. https://www.iagc.org/importance-of-fossil-fuels.html (accessed 31 December 2019).

23. Savage, S. Replacing Petro-chemicals With Bio-based Alternatives. Can We Do It? https://www.forbes.com/sites/stevensavage/2016/04/23/replacing-petro-chemicals-with-bio-based-alternatives-can-we-do-it/#4d4b66c539f5.
24. Contributors, I. Data and Statistics: Explore Energy Data by Category, Indicator, Country or Region. https://www.iea.org/data-and-statistics?country=WORLD (accessed 01 January 2020).
25. Contributors, B. *BP Statistical Review of World Energy*; British Petroleum: 2019.
26. Clark, D. Why we can't quit fossil fuels? https://www.theguardian.com/environment/2013/apr/17/why-cant-we-give-up-fossil-fuels (accessed 02 January 2020).
27. McGrath, M. Nuclear Fusion is 'a question of when, not if'. https://www.bbc.com/news/science-environment-50267017 (accessed 02 January 2020).
28. Leal, M. R. L.; Nogueira, L. A. H.; Cortez, L. A., Land demand for ethanol production. *Applied Energy* **2013,** *102*, 266-271.
29. Puttaiah, G.; Drennen, T. A.; Brunetti, S. C.; Traylor, C. M. In *Conversion of a Gasoline Internal Combustion Engine into a Hydrogen Engine*, American Society for Engineering Education, American Society for Engineering Education: 2012.
30. San Marchi, C.; Somerday, B. P., Technical reference on hydrogen compatibility ofmaterials. *Sandia National Laboratories, SANDIA REPORT SAND2008-1163* **2008**, 1211-1.
31. San Marchi, C.; Somerday, B. P.; Nibur, K. A., Development of methods for evaluating hydrogen compatibility and suitability. *International Journal of Hydrogen Energy* **2014,** *39*, 20434-20439.
32. Häussinger, P.; Lohmüller, R.; Watson, A. M., Hydrogen, 1. properties and occurence. *Ullmann's Encyclopedia of Industrial Chemistry* **2011**.
33. Milbrandt, A.; Mann, M. *Potential for Producing Hydrogen from Key Renewable Resources in the United States*; National Renewable Energy Lab.(NREL), Golden, CO (United States): 2006.
34. Wang, H., Solar Thermochemical Fuel Generation. In *Wind Solar Hybrid Renewable Energy System*, IntechOpen: 2020.
35. Steinfeld, A., Solar thermochemical production of hydrogen—a review. *Solar energy* **2005,** *78*, 603-615.
36. Sato, S., Thermochemical hydrogen production. *Solar-hydrogen energy systems* **1979**, 81-114.
37. Kalisman, P.; Nakibli, Y.; Amirav, L., Perfect photon-to-hydrogen conversion efficiency. *Nano letters* **2016,** *16*, 1776-1781.
38. Huya-Kouadio, J., Doe hydrogen and fuel cells program record. **2017**.
39. Burke, K. In *Unitized regenerative fuel cell system development*, 1st International Energy Conversion Engineering Conference (IECEC), 2003; p 5939.
40. Hu, M.; Triulzi, G.; Sharifzadeh, M., Technological change in fuel cell technologies. In *Design and Operation of Solid Oxide Fuel Cells*, Elsevier: 2020; pp 3-41.
41. Thomas, C., Fuel cell and battery electric vehicles compared. *international journal of hydrogen energy* **2009,** *34*, 6005-6020.
42. Bossel, U., Does a hydrogen economy make sense? *IEEE* **2006,** *94*, 1826-1837.
43. Nelson, D. L.; Lehninger, A. L.; Cox, M. M., *Lehninger principles of biochemistry*. Macmillan: 2008.
44. Raven, P. H.; Evert, R. F.; Eichhorn, S. E., *Biology of plants*. Macmillan: 2005.
45. Umena, Y.; Kawakami, K.; Shen, J. R.; Kamiya, N., Crystal structure of oxygen-evolving photosystem II at a resolution of 1.9 A. *Nature* **2011,** *473*, 55-60.

46. Suga, M.; Akita, F.; Hirata, K.; Ueno, G.; Murakami, H.; Nakajima, Y.; Shimizu, T.; Yamashita, K.; Yamamoto, M.; Ago, H.; Shen, J. R., Native structure of photosystem II at 1.95 Å resolution viewed by femtosecond X-ray pulses. *Nature* **2015,** *517*, 99-103.
47. Tsui, E. Y.; Kanady, J. S.; Agapie, T., Synthetic cluster models of biological and heterogeneous manganese catalysts for O_2 evolution. *Inorg. Chem.* **2013,** *52*, 13833-48.
48. Kanady, J. S.; Tsui, E. Y.; Day, M. W.; Agapie, T., A synthetic model of the Mn_3Ca subsite of the oxygen-evolving complex in photosystem II. *Science* **2011,** *333*, 733-736.
49. Zhang, C.; Chen, C.; Dong, H.; Shen, J.-R.; Dau, H.; Zhao, J., A synthetic Mn_4Ca-cluster mimicking the oxygen-evolving center of photosynthesis. *Science* **2015,** *348*, 690-693.
50. Dismukes, G. C.; Brimblecombe, R.; Felton, G. A.; Pryadun, R. S.; Sheats, J. E.; Spiccia, L.; Swiegers, G. F., Development of bioinspired Mn_4O_4− cubane water oxidation catalysts: lessons from photosynthesis. *Acc. Chem. Res.* **2009,** *42*, 1935-1943.
51. Carrell, T. G.; Cohen, S.; Dismukes, G. C., Oxidative catalysis by $Mn_4O_4^{6+}$ cubane complexes. *J. Mol. Catal. A: Chem.* **2002,** *187*, 3-15.
52. Ruettinger, W. F.; Campana, C.; Dismukes, G. C., Synthesis and Characterization of $Mn_4O_4L_6$ Complexes with Cubane-like Core Structure: A New Class of Models of the Active Site of the Photosynthetic Water Oxidase. *J. Am. Chem. Soc.* **1997,** *119*, 6670-6671.
53. Brousseau, L. C.; Williams, D.; Kouvetakis, J.; O'Keeffe, M., Synthetic Routes to Ga(CN)3 and MGa(CN)4 (M = Li, Cu) Framework Structures. *J. Am. Chem. Soc.* **1997,** *119*, 6292-6296.
54. Dasgupta, J.; Ananyev, G. M.; Dismukes, G. C., Photoassembly of the Water-Oxidizing Complex in Photosystem II. *Coord. Chem. Rev.* **2008,** *252*, 347-360.
55. Karkas, M. D.; Verho, O.; Johnston, E. V.; Akermark, B., Artificial photosynthesis: molecular systems for catalytic water oxidation. *Chem. Rev.* **2014,** *114*, 11863-2001.
56. Young, K. J.; Brennan, B. J.; Tagore, R.; Brudvig, G. W., Photosynthetic water oxidation: insights from manganese model chemistry. *Acc. Chem. Res.* **2015,** *48*, 567-74.
57. Lant, H. M.; Michaelos, T. K.; Sharninghausen, L. S.; Mercado, B. Q.; Crabtree, R. H.; Brudvig, G. W., N, N, O Pincer Ligand with a Deprotonatable Site That Promotes Redox-Leveling, High Mn Oxidation States, and a Mn2O2 Dimer Competent for Catalytic Oxygen Evolution. *European Journal of Inorganic Chemistry* **2019,** *2019*, 2115-2123.
58. Chaudhuri, P.; Wieghardt, K., The chemistry of 1, 4, 7-triazacyclononane and related tridentate macrocyclic compounds. *Prog. Inorg. Chem* **1987,** *35*, 329-436.
59. Barefield, E. K., Coordination chemistry of N-tetraalkylated cyclam ligands—A status report. *Coordination Chemistry Reviews* **2010,** *254*, 1607-1627.
60. Nath, B. D.; Takaishi, K.; Ema, T., Macrocyclic multinuclear metal complexes acting as catalysts for organic synthesis. *Catalysis Science & Technology* **2020**.
61. Atkins, P. W.; De Paula, J.; Keeler, J., *Atkins' physical chemistry*. Oxford university press: 2018.
62. Hamann, C. H.; Hamnett, A.; Vielstich, W., Electrochemistry. 2007. Weinheim: Wiley. XVIII.
63. McAuley, A.; Subramanian, S.; Barclay, T., Synthesis, structure and electrochemistry of isomeric nickel (II) complexes of a [9] ane fused cyclam macrotricycle: evidence for a stable trans-IV and a redox induced rearrangement in a trans-I conformation. *Dalton Transactions* **2010,** *39*, 9956-9961.

EXPERIMENTAL DATA

Abbreviations

Abbreviations of starting materials Common Name /IUPAC:

TACN	Triazacyclononane /1,4,7-Triazacyclononane
Cyclam	Tetraazacyclotetradecane /1,4,8,11-Tetraazacyclotetradecane
ClAcCl	Chloroacetyl chloride /2-Chloroacetyl chloride
DPA	2,2-Dipicolylamine /bis(pyridin-2-ylmethyl)amine
TMSOTf	TMS Triflate /trimethylsilyl trifluromethanesulfonate
$MnCl_2$	Manganese(II) chloride /manganese dichloride
$FeCl_2$	Iron(II) chloride /iron dichloride

Abbreviations of synthesized compounds Simple Name /Predicted IUPAC:

TACNAcCl	Triazacyclononaneacetyl Chloride /1,1',1"-(1,4,7-triazonane-1,4,7-triyl)tris(2-chloroethan-1-one)
TACNAcDPA	Triazacyclononaneacetyl-DPA /1,1',1"-(1,4,7-triazonane-1,4,7-triyl)tris(2-(bis(pyridin-2-ylmethyl)amino)ethan-1-one)
TACNAcDPA[Mn]	Triazacyclononaneacetyl-DPA Mn (Complex)
TACNAcDPA[Fe]	Triazacyclononaneacetyl-DPA Fe (Complex)
CyclamAcCl	Tetraazacyclotetradecaneacetyl-Chloride /1,1',1",1"'-(1,4,8,11-tetraazacyclotetradecane-1,4,8,11-tetrayl)tetrakis(2-chloroethan-1-one)
CyclamAcDPA	Tetraazacyclotetradecaneacetyl-DPA /1,1',1",1"'-(1,4,8,11-tetraazacyclotetradecane-1,4,8,11-tetrayl)tetrakis(2-(bis(pyridin-2-ylmethyl)amino)ethan-1-one)
CyclamAcDPA[Mn]	Tetraazacyclotetradecaneacetyl-DPA Mn (Complex)
CyclamAcDPA[Fe]	Tetraazacyclotetradecaneacetyl-DPA Fe (Complex)

$Mn(OTf)_2(CH_3CN)$	Manganese(II) triflate salt /$Mn(OTf)_2(CH_3CN)_2$
$Fe(OTf)_2(CH_3CN)$	Iron(II) triflate salt /$Fe(OTf)_2(CH_3CN)_2$

Abbreviations of solvents:

CH_3CN	Acetonitrile
$CHCl_3$	Chloroform
DCM	Dichloromethane
EtOAc	Ethyl acetate
MeOH	Methanol
DI-H_2O	Deionized Water
Hex	Hexane
Et_2O	Diethyl ether

Abbreviations of acids/bases:

Na_2CO_3	Sodium carbonate
Et_3N	Triethylamine
TMAOH	Tetramethylammonium hydroxide
Hunig's base	N,N-Diisopropylethylamine
HCL	Hydrochloric acid

Abbreviations for equipment:

RBF	Round-bottomed flask

NMR Abbreviation

s = singlet	dd = doublet of doublets	q = quartet	br = broad signal
d = doublet	dt = doublet of triplets	quint = quintet	
t = triplet	td = triplet of doublets	m = multiplet (denotes complex pattern)	

Overview of Metal Triflate Salts

Transition metal triflates were used as the source of metal ions in the synthesis of metal-ligand complexes. These were prepared in a nitrogen atmosphere glovebox at room temperature using the procedure described below.

The metal triflates synthesized in this work were manganese (II) triflate, $Mn(II)(OTf)_2(CH_3CN)_2$ and the iron (II) triflate, $Fe(II)(OTf)_2(CH_3CN)_2$.

Metal Triflate Synthesis

Synthesis of $Mn(II)(OTf)_2(CH_3CN)_2$. Inside an inert glovebox, 2.32 g of $MnCl_2$, 50 mL of anhydrous CH_3CN, 10 mL of Trimethylsilyl trifluoromethanesulfonate (TMSOTf) (new ampule, received commercially) and a stir bar were put to a 250 mL round bottom flask (RBF) with a side arm and a rubber septum on the top. The contents of the RBF were stirred. The TMSOTf was added last, slowly (30 to 60 sec.) using a syringe. This produced a turbid slurry that became warm to the touch. After 10 min., the solution homogenized into a clear pink color, and was left stirring for 24 hrs.

Next day, the solution appeared to have a yellowish-pink color. The solvent was removed under vacuum to dryness. The powdery residue was white in color with a slightly darker ring around the top of the substance.

The white residue was dissolved in anhydrous CH_3CN to give a dirty pink solution. The solution was filtered to remove any insoluble solid particles and was carefully layered with Et_2O. It was then placed inside the freezer (-35 ºC), and over the next day, a white precipitate was formed. The solvent was filtered off and the white precipitate was collected. The precipitate was thoroughly washed with Et_2O leaving a pure white powder. The filtrate solvent was reduced to a small volume using vacuum and layered with Et_2O to yield a second batch of white powder.

Synthesis of $Fe(II)(OTf)_2(CH_3CN)_2$. The iron triflate was produce in the same way using $FeCl_2$. The cloudy slurry went to a clear purple color solution at the beginning, but the color changed to yellowish-purple the next morning. After the powder was dissolved in anhydrous CH_3CN, it gave a dirty green colored solution. Finally, after the Et_2O layer/wash, the precipitate was also a pure white powder.

Synthesis of the Ligands

Synthesis of 1,1',1''-(1,4,7-triazonane-1,4,7-triyl)tris(2-chloroethan-1-one), TACNAcCl

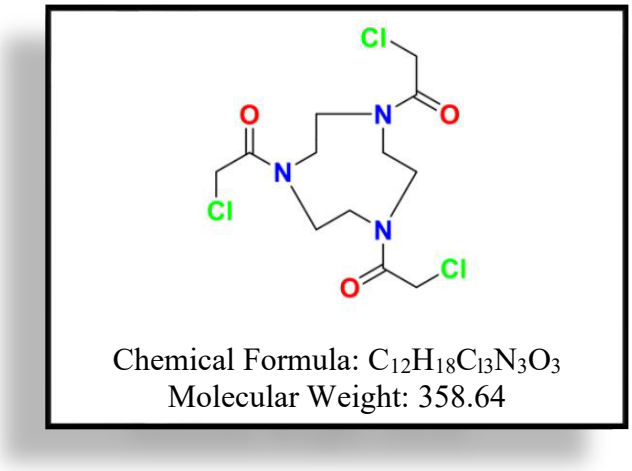

Chemical Formula: $C_{12}H_{18}C_{l3}N_3O_3$
Molecular Weight: 358.64

This procedure was adapted from McAuley et al.[63]. 1.80 grams of TACN was dissolved in 200 mL of $CHCl_3$ in a 500 mL three-necked round-bottomed flask (RBF) equipped with a stir bar and rubber septum on both outer necks. An addition funnel was secured on the central neck. The RBF was wrapped in foil to prevent unwanted photochemical reactions. It was then placed in an ice bath (salted with NaCl) to bring the temperature down below 0 ºC. This temperature, ~ -10 ºC, was maintained throughout the addition of the reagents (~70 min. before the temperature rose slowly to room temperature).

The addition funnel was charged with a solution of 4.5 eqv. (5.00 mL) of chloroacetyl chloride (ClAcCl) dissolved in 40 mL of $CHCl_3$. This was added dropwise to the reaction flask

over a 40-minute period. After the first quarter was added (10 mL ClAcCl over 10 min.), one quarter of prepared base (Na_2CO_3 dissolved in 20 mL water) was injected using a syringe. It was added to the reaction flask (~5 mL at a time) after every quarter addition of ClAcCl solution. Once all additions were complete, the reaction mixture was left stirring at room temperature (22 ºC) overnight.

Next day, the reaction mixture was added to a separatory funnel. The reaction flask was rinsed with 10 mL to 20 mL of DI-H_2O that was also added to the separatory funnel and was separated from the organic layer.

The organic layer was washed with 20 mL of fresh DI-H_2O. (If Et_3N is used as a base, the mixing was done very slowly, because quick mixing produces black solids that are tough to remove, and it traps product.) The organic layer was separated, dried using sodium sulfate, filtered and evaporated to 50 to 75 mL. This was then diluted with hexane, and a white precipitate (brown if Et_3N was used as a base) fell out of solution (3.36g). The precipitate was filtered. The hexane layer was evaporated to 50 mL and diluted again producing more precipitate (400 mg) which was added to the original collection. The aqueous layer was acidified and extracted from DCM giving a further 400 mg. This results in an overall ~84% yield. Further purification can be accomplished by column chromatography using basic alumina as the stationary phase (Al_2O_3, CAS: 1344-26-1). The mobile phase included hexane as the starting solvent followed by EtOAc mixture, increasing the polarity to 100% EtOAc. Then finally to no more than 95:5: EtOAc:MeOH. However, this is not necessary when Na_2CO_3 is used as a base due to the high purity of the product. ^{1}H-NMR (300 MHz, $CDCl_3$ 7.26) δ 4.10 (s, 6H), 3.78 (t, 6H), 3.58 (t, 6H); ^{13}C-NMR (300 MHz, CD_3CN 118.26) δ 168.73 (C=O), 51.83 (CH_2), 49.29 (CH_2), 43.08 (CH_2); IR (solid) 2359, 2337, 1643, 1460, 1410, 1364, 1220, 1184, 1135, 1090, 1034, 794, 727, 667, 650, 570 cm^{-1}.

Synthesis of 1,1',1''-(1,4,7-triazonane-1,4,7-triyl)tris(2-(bis(pyridin-2ylmethyl)amino)ethan-1-one), TACNAcDPA

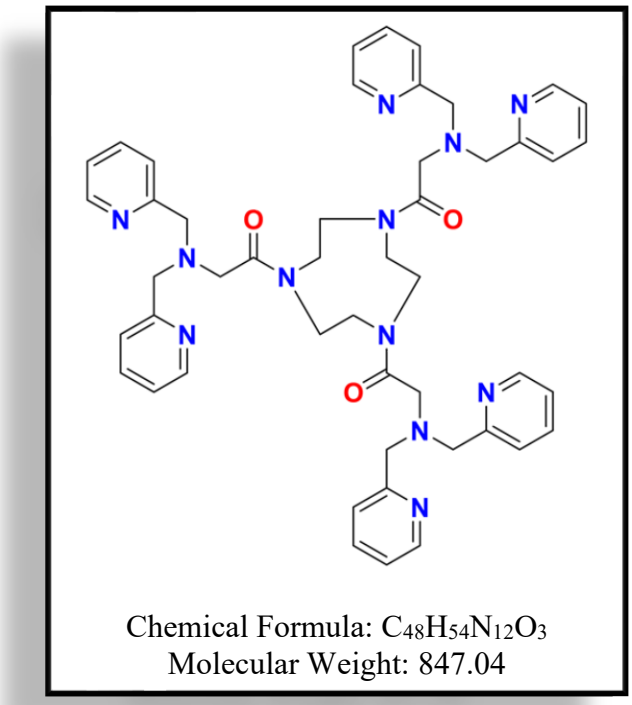

Chemical Formula: $C_{48}H_{54}N_{12}O_3$
Molecular Weight: 847.04

3.28 grams of TACNAcCl, 25 mL CH_3CN, 6 eqv. (5.82 g) Na_2CO_3 and a stir bar was added to a 50 mL three neck RBF. The side necks of the RBF were sealed with rubber septum and the central neck received a reflux condenser with N_2 flow. This was placed in an oil bath preset at a temperature of ~90 ºC. Stirring was started and maintained at full speed to keep the Na_2CO_3 suspended. 4 eqv. (6.58 mL) of DPA was added using a syringe, and the reaction mixture was refluxed at ~90 ºC for 24 hrs.

Next day, the reaction was stopped and the Na_2CO_3 settled to the bottom revealing a pale-yellow to orange solution. The reaction mixture was filtered using a fritted filter to remove solid Na_2CO_3. The filtered solid and reaction flask were further washed with CH_3CN and added to the filtrate. The filtered solution was evaporated completely, dissolved in DCM and washed with acidic DI-H_2O. The organic layer was dried using Na_2SO_4, filtered and evaporated completely. A

dark caramel-red colored sticky solid was obtained. It was further dissolved in EtOAc, filtered and evaporated. It was then dissolved in a small amount of DCM and diluted with hexane and stirred for an hour. This step will remove a large portion of unreacted DPA into the hexane layer.

The hexane is decanted, and the remaining substance is evaporated completely to a gel-like substance of a very dark-red color (7.54 g, 97% recovery).

Further purification can be accomplished by column chromatography using basic alumina as the stationary phase (Al_2O_3, CAS: 1344-26-1). The mobile phase included hexane as a starting solvent. The mobile phase was changed to 100% EtOAc until all DPA is removed. Then the polarity was increased slowly using MeOH, and finally no more than 95:5, EtOAc:MeOH. After the column, the product obtained was a bright, pinkish-orange, popped rice-like, sticky substance (this reduces the yield to 86%). ^{1}H-NMR (300 MHz, $CDCl_3$ 7.26) δ 8.50 (d, 6H),7.61 (td, 6H), 7.42 (d, 6H),7.12 (td, 6H), 3.86 (s, 12H), 3.54 (m, 6H), 3.31 (s, 6H), 3.20 (m, 6H).; ^{13}C-NMR (300 MHz, $CDCl_3$ 77.16) δ 171.61 (C=O), 158.81 (C), 149.16 (CH), 136.64 (CH), 123.65 (CH), 122.35 (CH), 60.39 (CH_2), 56.40 (CH_2), 51.24 (CH_2), 48.26 (CH_2); IR (solid) 2359, 2340, 1638, 1594, 1476, 1460, 1432, 761, 677, 668, 647 cm^{-1}.

Synthesis of 1,1',1'',1'''-(1,4,8,11-tetraazacyclotetradecane-1,4,8,11-tetrayl)tetrakis(2-chloroethan-1-one), CyclamAcCl

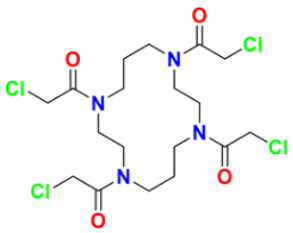

Chemical Formula: $C_{18}H_{28}Cl_4N_4O_4$
Molecular Weight: 506.25

This procedure was adapted from McAuley et al.[63] 2.0 grams of cyclam was dissolved in 200 mL of $CHCl_3$ in a 500 mL three-necked RBF equipped with a stir bar and rubber septum on both side necks. An addition funnel was secured on the central neck and a pressure release system was secured onto the top of the addition funnel. The RBF was wrapped in foil to prevent any photo-dissociative reactions. It was then placed in an ice bath (salted with NaCl) to bring the temperature below 0 ºC. This temperature (~ -10 ºC) was maintained throughout the addition of the reagents (~70 min., before the temperature slowly warmed up to room temperature).

The addition funnel was charged with a solution of 6 eqv. (4.76 g) ClAcCl dissolved in 40 mL of $CHCl_3$. This was added dropwise to the reaction flask over a 40-minute period. After the first quarter was added (10 mL ClAcCl over 10 min.), one quarter of a prepared base was injected using a syringe. The base was prepared using 8 eqv. (8.47 g) Na_2CO_3 dissolved in 20 mL of DI-H_2O, and it was added to the reaction flask (5 mL at a time) after every quarter of ClAcCl addition. Once all additions were complete, the reaction mixture was left stirring at room temperature (22 ºC) overnight.

Next day, the reaction mixture was added to a separatory funnel. The reaction flask was rinsed with a few mL of DI-H_2O. This was also added to the separatory funnel. There was a white solid/foamy looking layer floating on the aqueous layer.

The organic layer was separated and washed using 20 mL of DI-H_2O. It was then dried using sodium sulfate, filtered and evaporated to ~ 50-75 mL. This was then diluted with hexane, and a yellowish-white gel formed at the bottom. The hexane layer was decanted. The gel was dissolved in DCM and evaporated several times to remove the remaining hexane (4.46 g). This resulted in ~88% yield of the desired compound and was pure enough (by ^{1}H-NMR) for the next reaction. Further purification can be accomplished by column chromatography using basic alumina

as the stationary phase (Al_2O_3 CAS: 1344-26-1). Mobile phase included hexane starting solvent with gradual increase in EtOAc followed by MeOH, and finally no more than 90:10, EtOAc:MeOH. The final substance bubbles up while drying under vacuum. This produced a white, sticky, popped rice-like material. ^{1}H-NMR (300 MHz, $CDCl_3$ 7.26) δ ppm 4.21, 4.10 (s, 8H), 3.66, 3.52 (m, 8H), 2.04 (p, 4H). ^{13}C-NMR (300 MHz, CD_3CN 118.26) δ 167.72 (C=O), 55.27 (CH_2), 47.90 (CH_2), 42.46 (CH_2), 28.33 (CH_2); IR (solid) 2364, 2352, 2159, 1644, 1452, 667 cm^{-1}.

Synthesis of 1,1',1'',1'''-(1,4,8,11-tetraazacyclotetradecane-1,4,8,11-tetrayl)tetrakis(2-(bis(pyridin-2-ylmethyl)amino)ethan-1-one), CyclamAcDPA

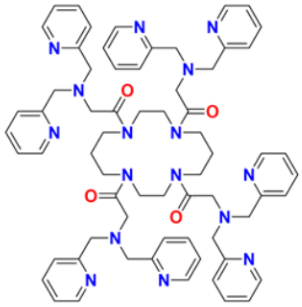

Chemical Formula: $C_{66}H_{76}N_{16}O_4$
Molecular Weight: 1157.41

1.91 gram of CyclamAcCl, 30 mL CH_3CN, 8 eqv. (3.20 g) Na_2CO_3 and a stir bar were added to a 100 mL three-necked RBF. The side necks were sealed with rubber septum and the central neck received a reflux condenser with N_2 flow. This was placed in an oil bath preset at a temperature of 90ºC. Stirring was started and maintained at full speed to keep the Na_2CO_3 suspended. 4.25 eqv. (2.89 mL) of DPA was added using a syringe, and the reaction mixture was refluxed at ~90ºC for 24 hrs.

When the reaction was stopped the next day, the Na_2CO_3 settled to the bottom. The reaction mixture was filtered using a fritted filter. The solids and reaction flask were further washed with

CH_3CN and added to the filtrate. The filtered solution was evaporated completely. A dark semi-orange, amber-colored, sticky substance remained. It was then dissolved in a small amount of DCM and diluted with hexane and stirred for an hour. This step removed a large portion of unreacted DPA into the hexane layer.

The hexane was decanted, and the remaining compound was evaporated completely to a gel-like substance of a very dark-red color. This substance was dissolved in EtOAc, and a black precipitate formed that contained a small amount of product and large portion of a compound that is not visible on ^{1}H-NMR. The EtOAc-soluble compound, once evaporated, has a less dark-red color. This exhibited some popped rice-like behavior (3.2 g, yield = 73%). ^{1}H-NMR (300 MHz, $CDCl_3$) δ 8.48 (dd, 4H), 7.59 (ddd, 4H), 7.11 (m, 8H), 3.92 (m, 16H), 3.62 (s, 8H), 3.45 (m, 8H), 3.36 (m, 8H), 1.65 (p, 4H); ^{13}C-NMR (300 MHz, $CHCL_3$ 77.16) δ 170.80 (C=O), 159.29 (CH_2), 148.95 (CH_2), 136.44 (CH_2), 123.58 (CH_2),122.30 (CH_2), 60.24 (CH_2), 55.02, 46.52 (CH_2), 44.93 (CH_2), 27.98 (CH_2); IR (solid) 2362, 2344,1636, 1591,1568, 1473, 1431, 768, 667 cm^{-1}.

Synthesis of Metal-Ligand Complexes

Synthesis of $Mn(II)_3(L)(OTf)_6$, L = 1,1',1''-(1,4,7-triazonane-1,4,7-triyl)tris(2-(bis(pyridin-2-ylmethyl)amino)ethan-1-one, TACNAcDPA)

Inside an inert gas glovebox, 140 mg of TACNAcDPA ligand was dissolved in 5 mL CH_3CN in a 20 mL scintillation vial equipped with a stir bar. To this, 3.2 eqv. (230 mg) of $Mn(II)(OTf)_2(CH_3CN)_2$, dissolved in 5 mL of CH_3CN was added and the vial was capped (total volume = 10 mL). The reaction mixture was stirred overnight to get a brownish-orange solution.

The reaction mixture was filtered to remove any solid impurity, evaporated to ~5 mL and added to a new scintillation vial. The solution was carefully layered with 5 mL Et_2O and placed in the freezer for several days. A white/brownish-orange solid precipitated. The liquid was decanted,

and the solid was collected and dried. Again, CH_3CN was added to the solid, and the solution was layered with Et_2O, capped, and returned to the freezer for recrystallization. Days later, the liquid was decanted leaving a brownish-orange to white substance (224 mg) for a 71% recovery. No crystals were obtained. ^{1}H-NMR (300 MHz, $CDCl_3$) δ ppm 55.17, 6.90, 5.18, 3.16, 2.88, 1.98, 0.99, 0.86, 0.69, -2.48, -13.09; IR (solid) 3433 (b), 2356, 2336, 1603, 1491, 1446, 1281, 1247, 1227, 1156, 1096, 1029, 767, 668, 632, 579,520 cm^{-1}.

Synthesis of $Fe(II)_3(L)(OTf)_6$, L = 1,1',1''-(1,4,7-triazonane-1,4,7-triyl)tris(2-(bis(pyridin-2-ylmethyl)amino)ethan-1-one, TACNAcDPA)

Inside an inert gas glovebox, 170 mg of TACNAcDPA ligand was dissolved in 5 mL DCM in a 20 mL scintillation vial equipped with a stir bar. To this, 3.2 eqv. (280 mg) of $Fe(II)(OTf)_2(CH_3CN)_2$, dissolved in 5 mL of DCM (slurry) was added, and the vial was capped. The solution immediately turned dark brown in color. The mixture was left stirring overnight. Next day, the solution had a green tint.

The reaction mixture was filtered, evaporated to ~5 mL and added to a crystallization chamber consisting of an open 20 mL scintillation vial containing the reaction mixture inside a larger vessel containing Et_2O. The chamber was sealed and left on a shelf in the glovebox for several days. The product produced was a white/dirty-brownish-green solid (336 mg) with an 88% recovery. No crystals were obtained. ^{1}H-NMR (300 MHz, CD_3CN) δ ppm 52.74, 17.91, 12.71, 7.61, 5.47, 3.43, 2.78, 1.96, 1.15; IR (solid) 3335 (b), 2365, 2345, 1628 cm^{-1}.

Synthesis of $Mn(II)_4(L)(OTf)_8$, L = 1,1',1'',1'''-(1,4,8,11-tetraazacyclotetradecane-1,4,8,11-tetrayl)tetrakis(2-(bis(pyridin-2-ylmethyl)amino)ethan-1-one, CyclamAcDPA)

Inside an inert gas glovebox, 200 mg of CyclamAcDPA ligand was dissolved in 5 mL CH_3CN in a 20 mL scintillation vial equipped with a stir bar. To this, 4.2 eqv. (316 mg) of

$Mn(II)(OTf)_2(CH_3CN)_2$, dissolved in 5 mL of CH_3CN was added and the vial was capped. The ligand solution was pink to start with but turned a clear dark orange instantly when the triflate was added. The solution had not changed the next day. (*When DCM was used as a solvent: A fewmin. after addition of manganese triflate the solution began turning a neon orange. 20 min. later it had a milky orange color, and after three hours a clear dark orange solution remained. The mixture was left stirring overnight. The next day the solution was a semi cloudy orange color appearing to have two layers*.)

The reaction mixture was filtered, evaporated to ~5 mL and added to a new scintillation vial. The solution was carefully layered with 5 mL Et_2O and placed in the freezer for several days. A white/faint-pink solid precipitated from the solution. The liquid was decanted, and the solid was collected and dried. Again, CH_3CN was added to the vial. This pulled the pink color out? but did not dissolve the solid. This solvent was immediately decanted and CH_3CN was added to the solid. It took just over a minute to dissolve. The solution was layered with Et_2O, capped and returned to the freezer. Days later, the liquid was decanted to find a pinkish white solid. The solid was dried on high vacuum and weighed (276 mg), for a recovery of 62%. ^{1}H-NMR (300 MHz, CD_3CN) δ ppm 5.32, 3.30, 1.97, 1.00; IR (solid) 2363, 2336, 1611, 1248, 1169, 1025, 759, 675, 667, 645 cm^{-1}.

Synthesis of $Fe(II)_4(L)(OTf)_8$, L = 1,1',1'',1'''-(1,4,8,11-tetraazacyclotetradecane-1,4,8,11-tetrayl)tetrakis(2-(bis(pyridin-2-ylmethyl)amino)ethan-1-one, CyclamAcDPA)

Inside an inert gas glovebox, 203 mg of CyclamAcDPA ligand was dissolved in 5 mL CH_3CN in a 20 mL scintillation vial equipped with a stir bar. To this, 4.2 eqv. (321 mg) of $Fe(II)(OTf)_2(CH_3CN)_2$, dissolved in 5 mL of CH_3CN (slurry) was added and the vial was capped. The solution started pink from the ligand, but within a few minutes after addition of iron triflate,

the solution turned brown. The mixture was left stirring overnight. Next day, the solution was found green in color.

The reaction mixture was filtered, evaporated to ~5 mL and added to a crystallization chamber consisting of an open 20 mL scintillation vial containing the reaction mixture inside a larger vessel containing Et_2O. The chamber was sealed and left on a shelf in the glovebox for several days. The product produced was a white/dirty-green solid. The remaining liquid was decanted, and the crystals were dried on high vacuum (356 mg) for a 79% recovery. ^{1}H-NMR (300 MHz, CD_3CN) δ ppm 123.38, 116.22, 72.32, 67.39, 61.24, 59.55, 54.92, 53.95, 53.02, 52.47, 52.18, 51.21, 50.53, 44.76, 42.23, 40.34, 16.60, 15.98, 15.55, 14.90, 14.26, 12.10, 11.66, 10.62, 9.68, 6.55, 5.44, 3.35, 2.05, 1.84, 1.15, -0.76, -1.01, -1.98, -6.23, -6.44, -6.95, -8.10, -8.86; IR (solid) 2365, 2344, 1608, 1256, 1171, 1033, 768, 683, 668, 652 cm^{-1}.

LIST OF APPENDICES

Tables

Table 1: Summary of Synthesized Compounds and Their Yields

Compound	Yield
TACNAcCl	84%
TACNAcDPA	86%
$Fe(II)_3(L)(OTf)_6$, L =TACNAcDPA	88%
$Mn(II)_3(L)(OTf)_6$, L =TACNAcDPA	71%
CyclamAcCl	88%
CyclamAcDPA	73%
$Fe(II)_4(L)(OTf)_8$, L = CyclamAcDPA	79%
$Mn(II)_4(L)(OTf)_8$, L = CyclamAcDPA	62%

Data Sets:

Data Set 1.1.1: ^{1}H-NMR of TACNAcCl recorded in $CDCl_3$ at 298 K

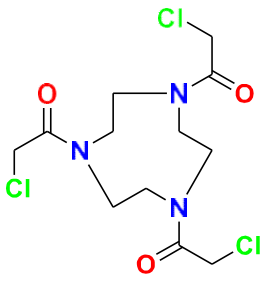

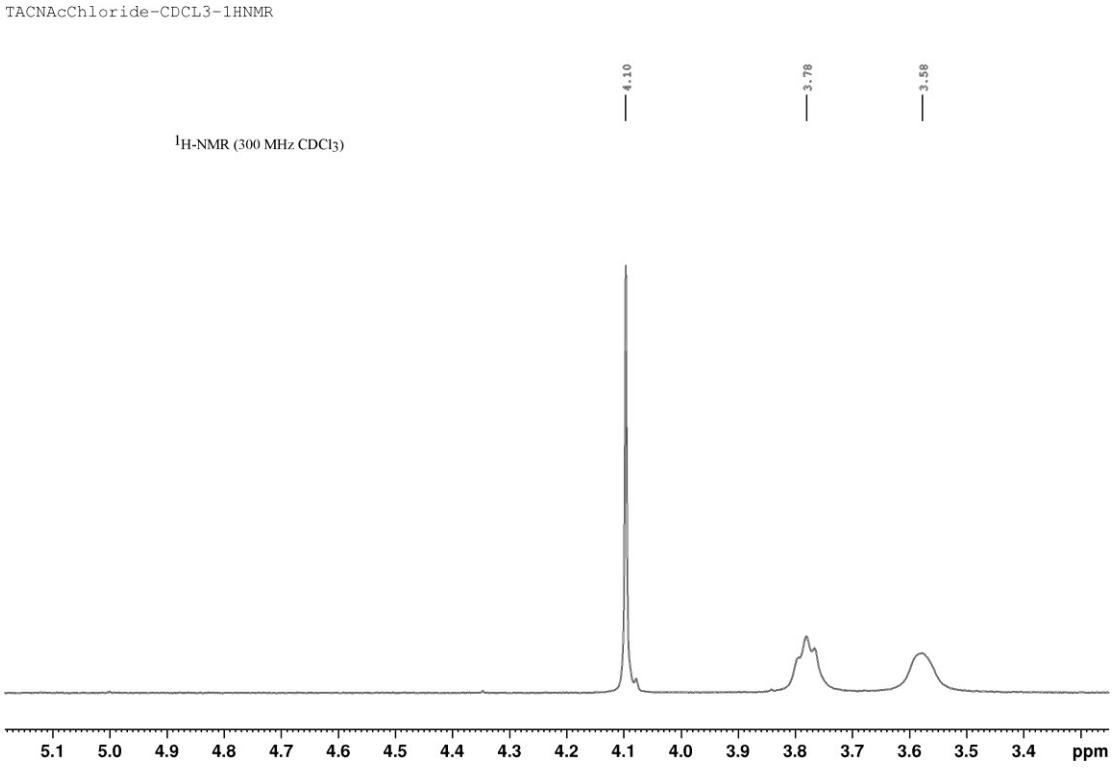

Data Set 1.1.2: ^{13}C-NMR of TACNAcCl recorded in CD_3CN at 298 K

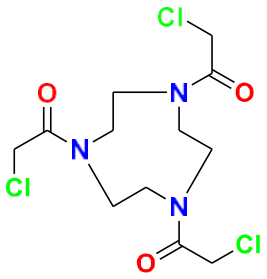

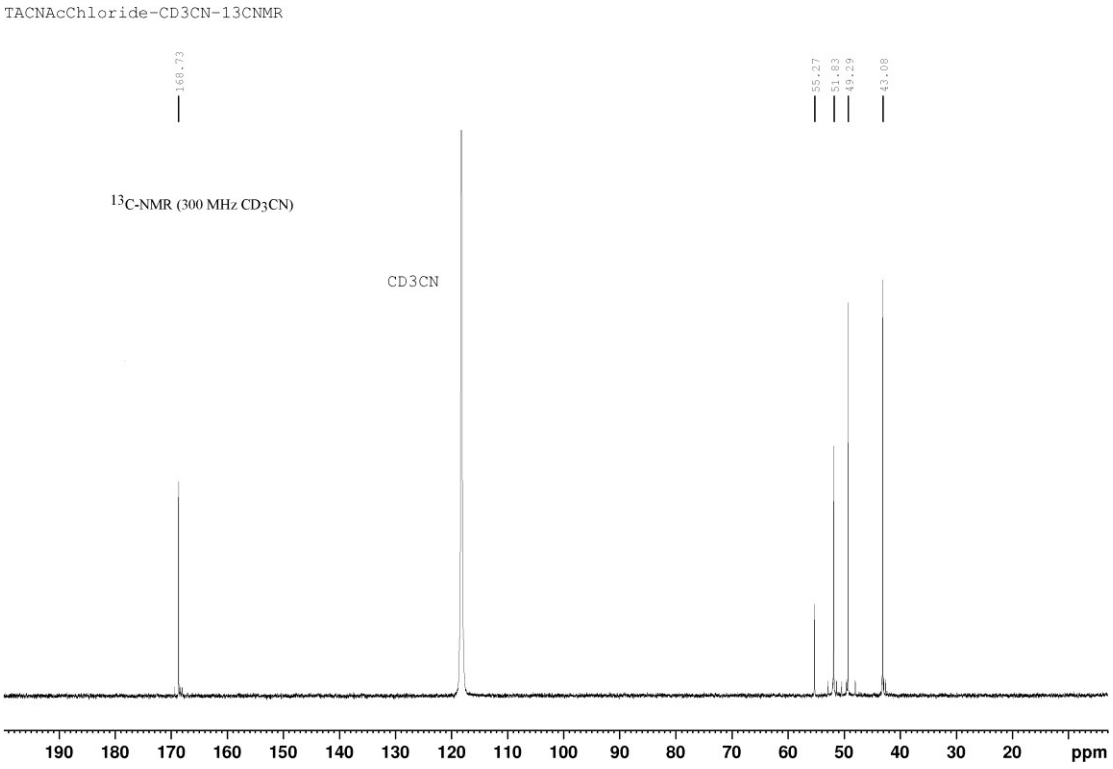

Data Set 1.1.3: FT-IR of solid TACNAcCl collected at 298 K on Thermo Scientific, Nicolet iS5 (iD7-ATR)

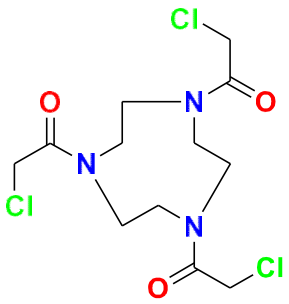

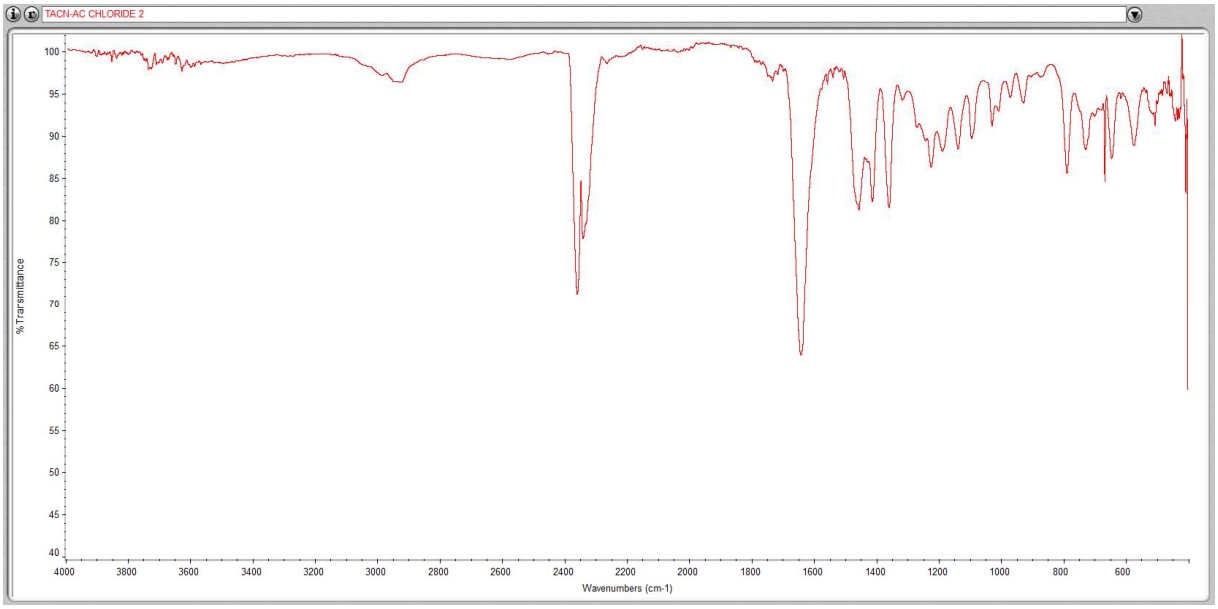

Data Set 1.2.1: ^{1}H-NMR of TACNAcDPA recorded in $CDCl_3$ at 298 K

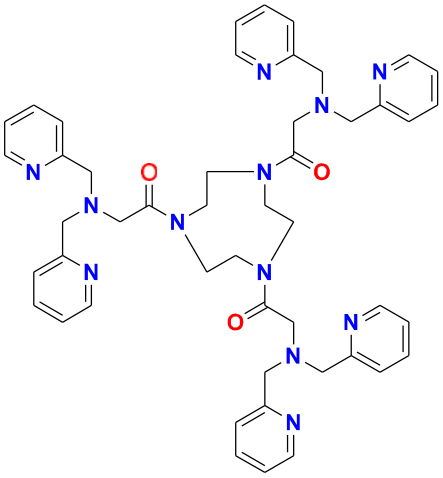

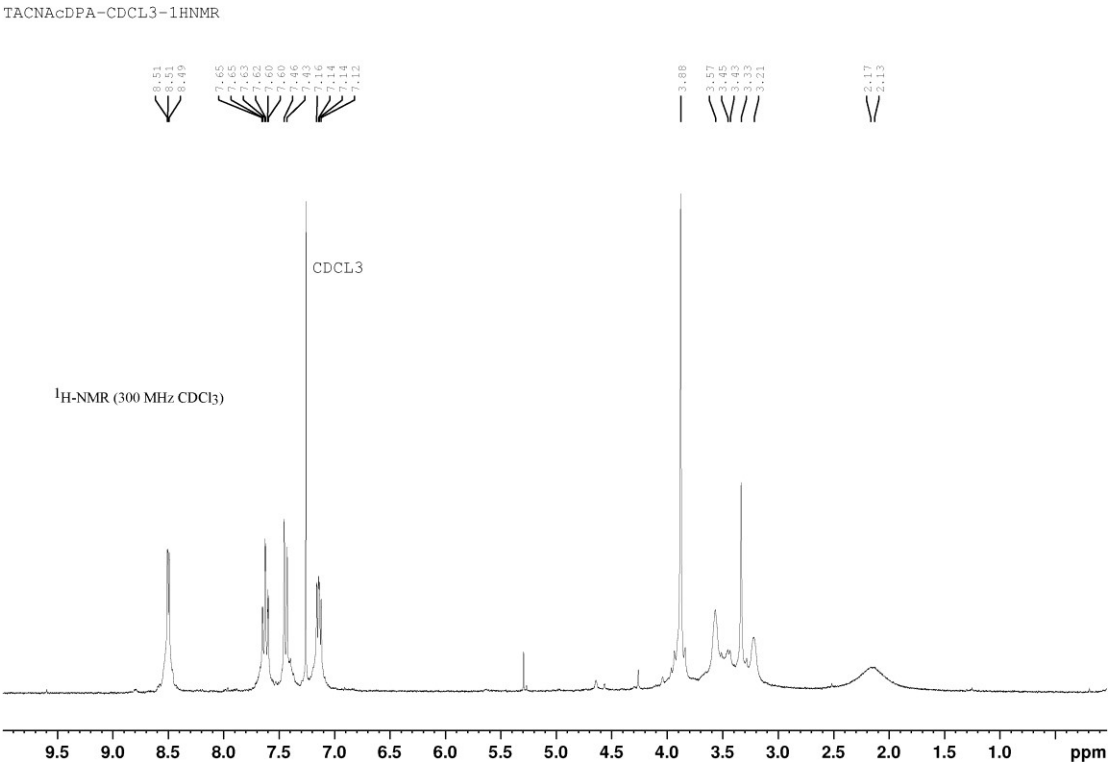

Data Set 1.2.1: ^{13}C-NMR of TACNAcDPA recorded in $CDCl_3$ at 298 K

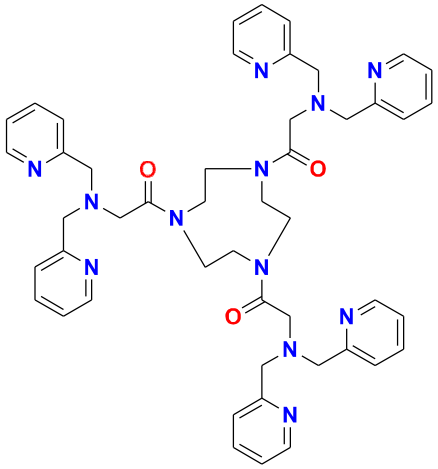

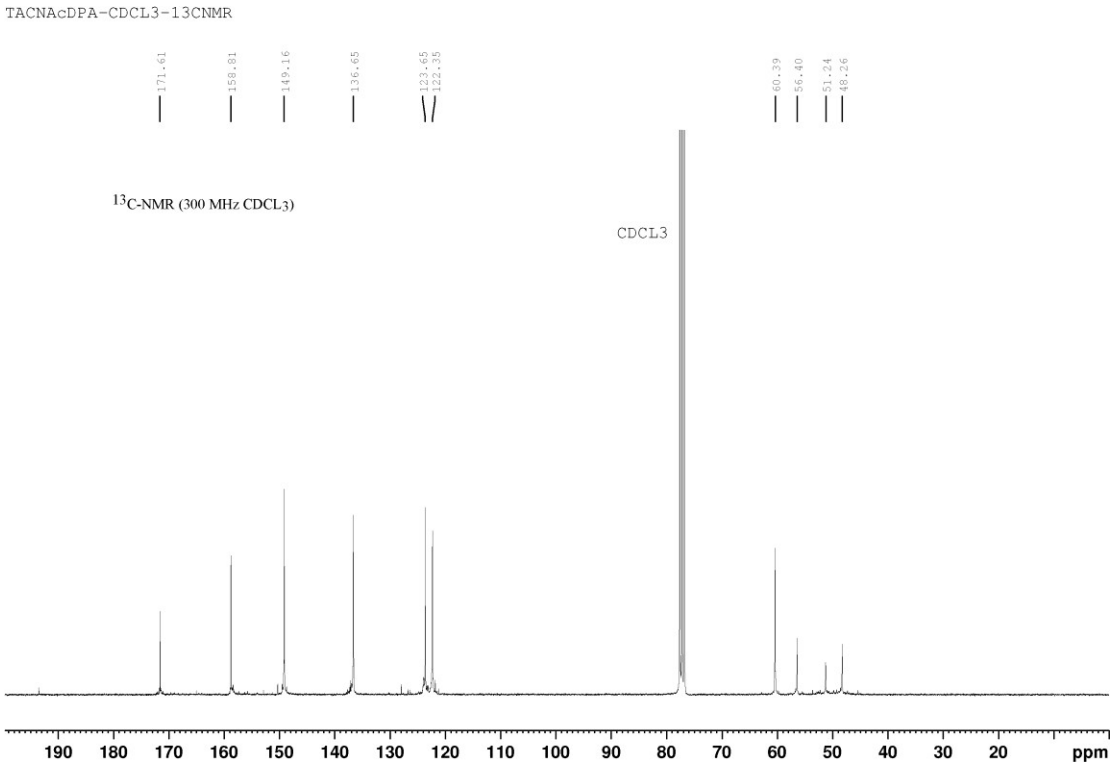

Data Set 1.2.3: FT-IR of solid TACNAcDPA collected at 298 K on Thermo Scientific, Nicolet iS5 (iD7-ATR)

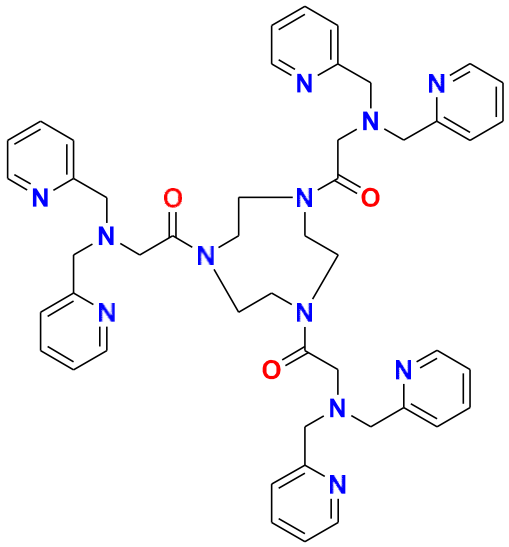

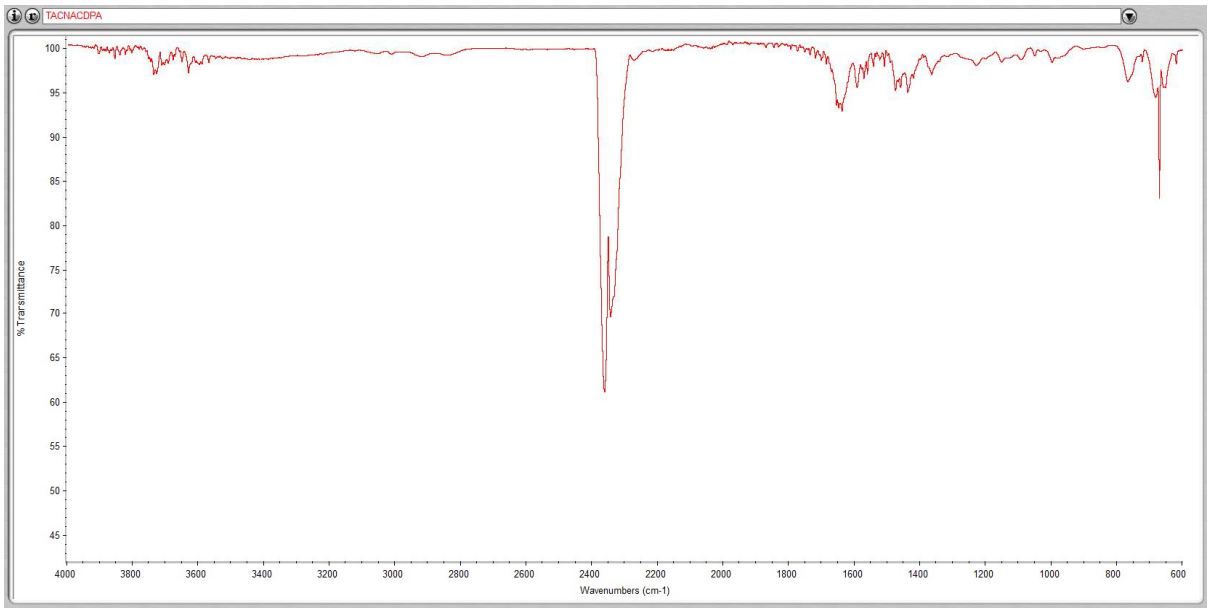

Data Set 1.3.1: ^{1}H-NMR of Mn(II)$_3$(L)(OTf)$_6$, L = TACNAcDPA, recorded in CD$_3$CN at 298 K

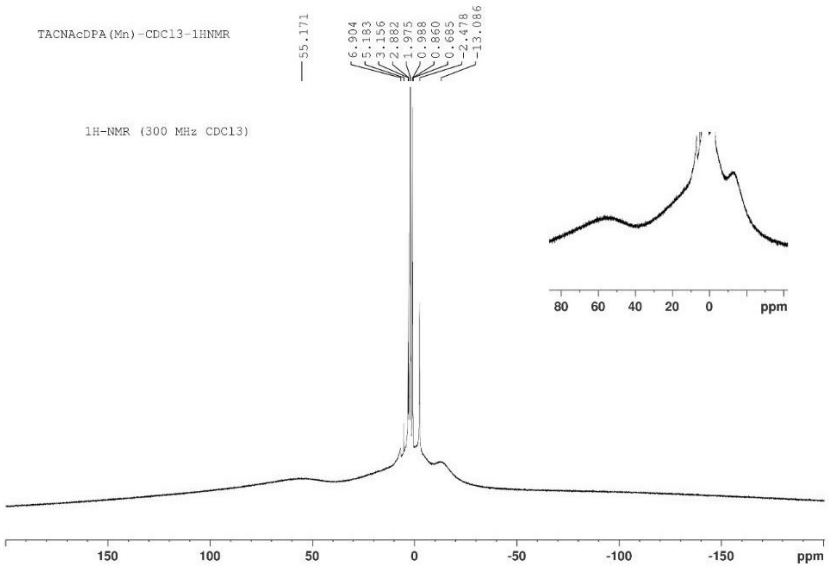

Data Set 1.3.2: UV-Vis absorption spectrum of Mn(II)$_3$(L)(OTf)$_6$, L = TACNAcDPA, recorded in CH$_3$CN at 298 K

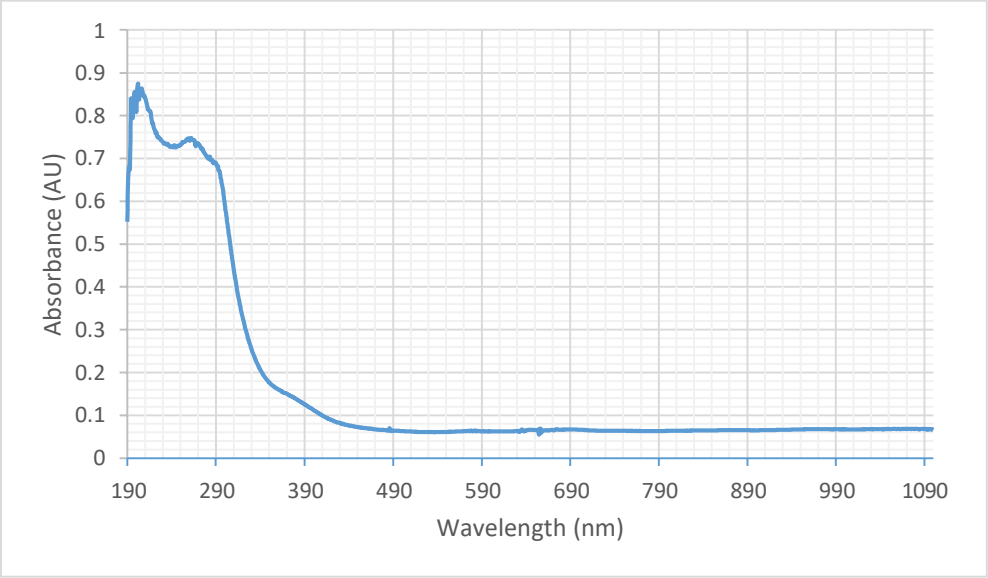

Data Set 1.3.3: FT-IR of solid $Mn(II)_3(L)(OTf)_6$, L = TACNAcDPA collected at 298 K on Thermo Scientific, Nicolet iS5 (iD7-ATR)

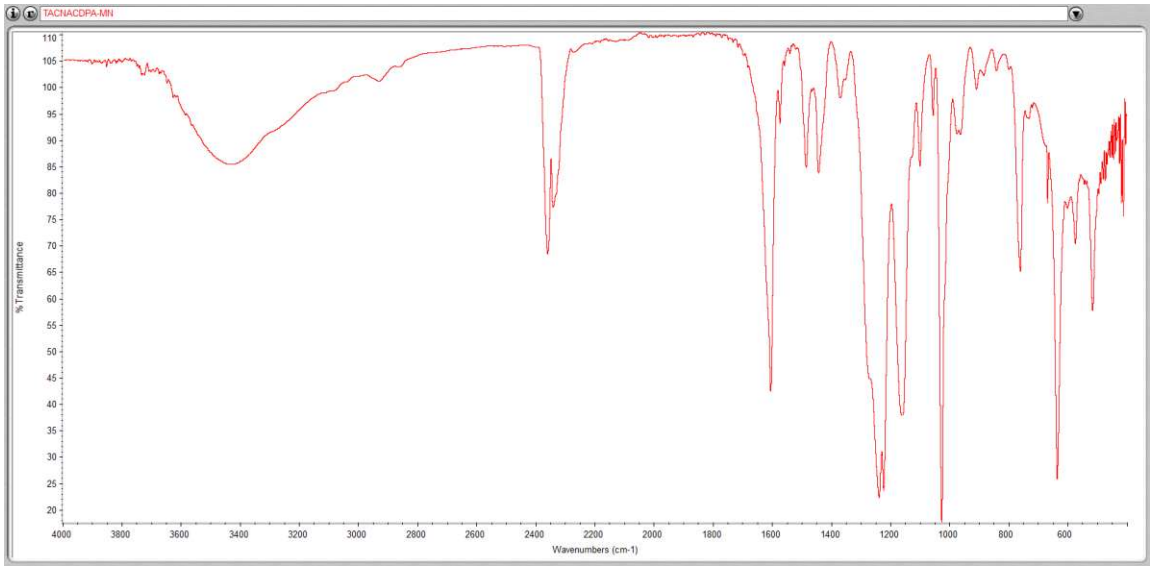

Data Set 1.4.1: ^{1}H-NMR of $Fe(II)_3(L)(OTf)_6$, L = TACNAcDPA, recorded in CD_3CN at 298 K

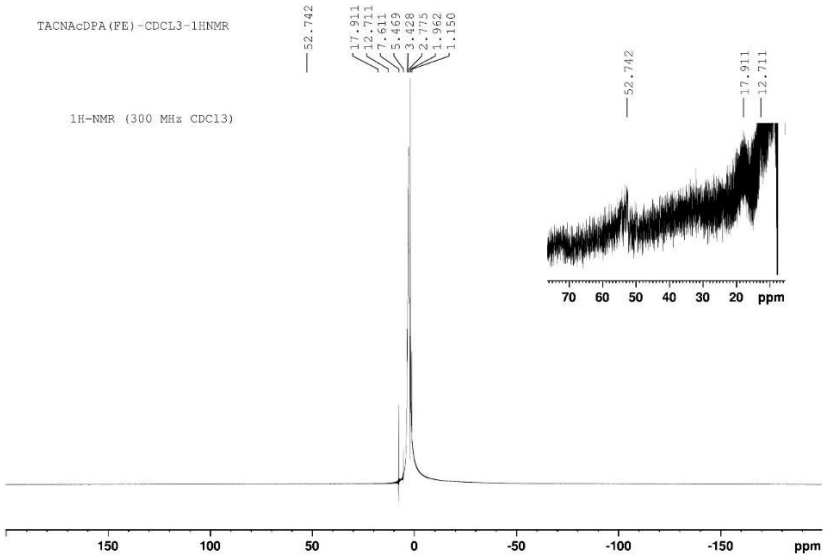

Data Set 1.4.2: UV-Vis absorption spectrum of $Fe(II)_3(L)(OTf)_6$, L = TACNAcDPA, recorded in CH_3CN at 298 K

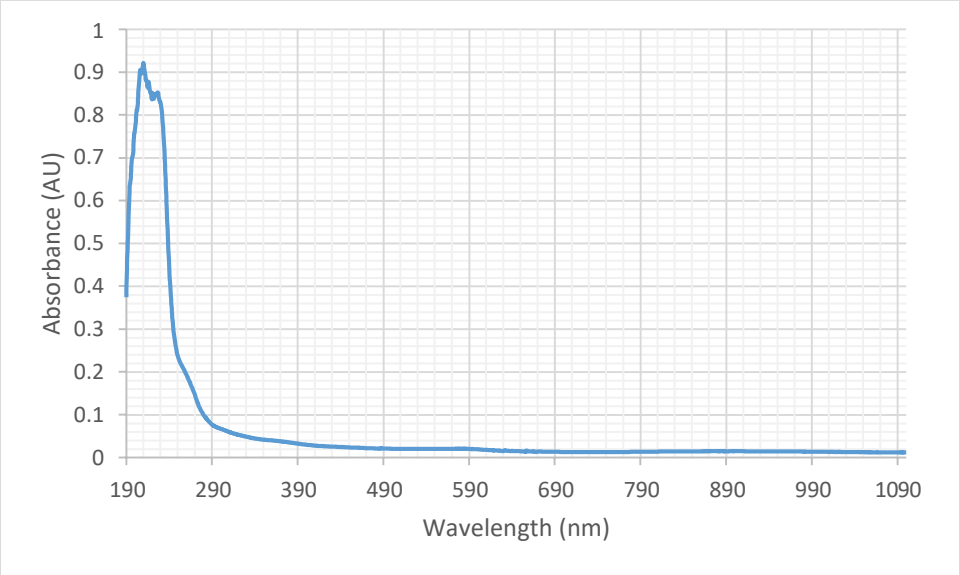

Data Set 1.4.3: FT-IR of solid $Fe(II)_3(L)(OTf)_6$, L = TACNAcDPA collected at 298 K on Thermo Scientific, Nicolet iS5 (iD7-ATR)

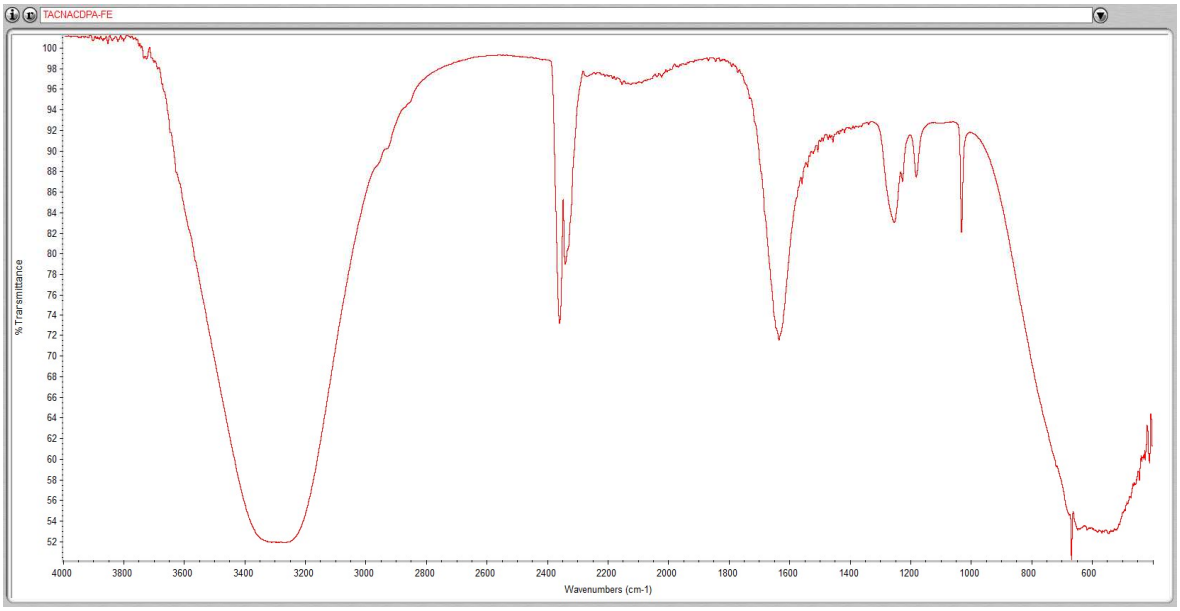

Data Set 2.1.1: ^{1}H-NMR of CyclamAcCl recorded in $CDCl_3$ at 298 K

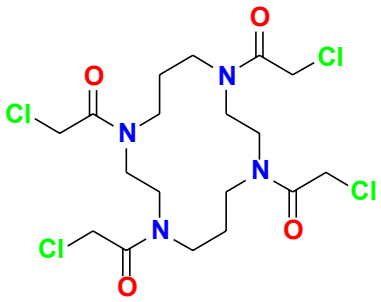

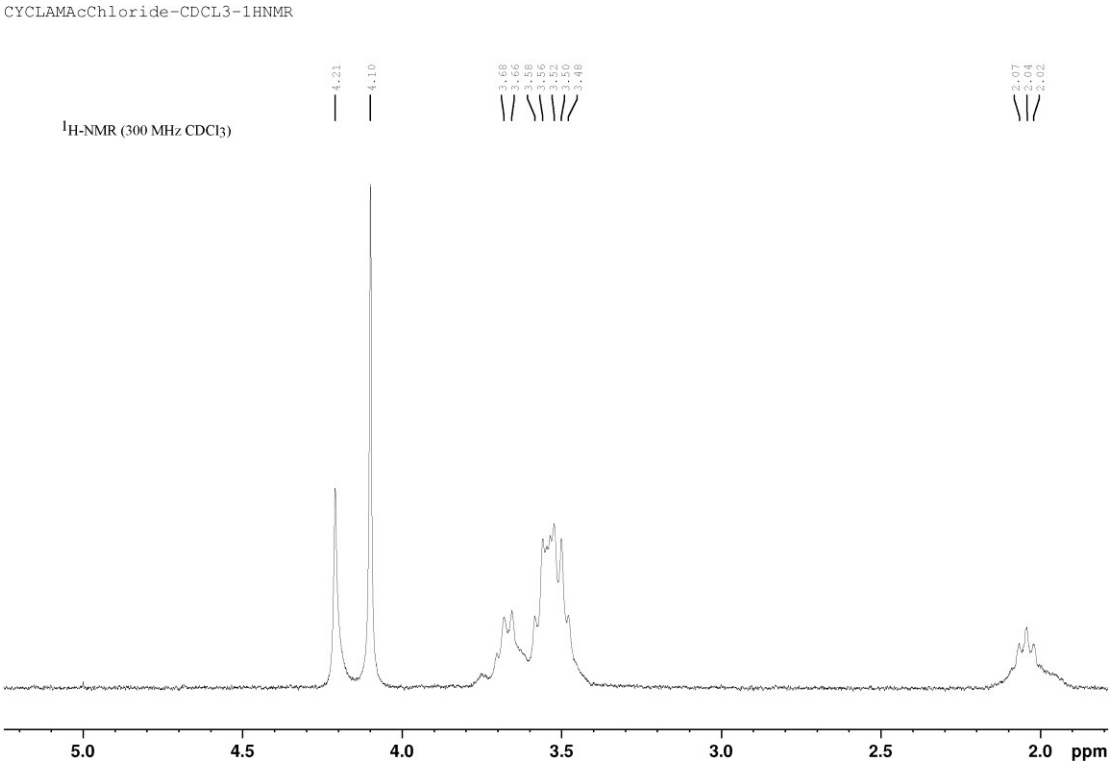

Data Set 2.1.2: 13C-NMR of CyclamAcCl recorded in CD_3CN at 298 K

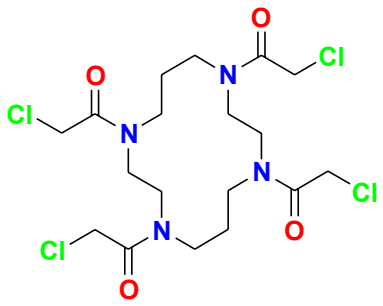

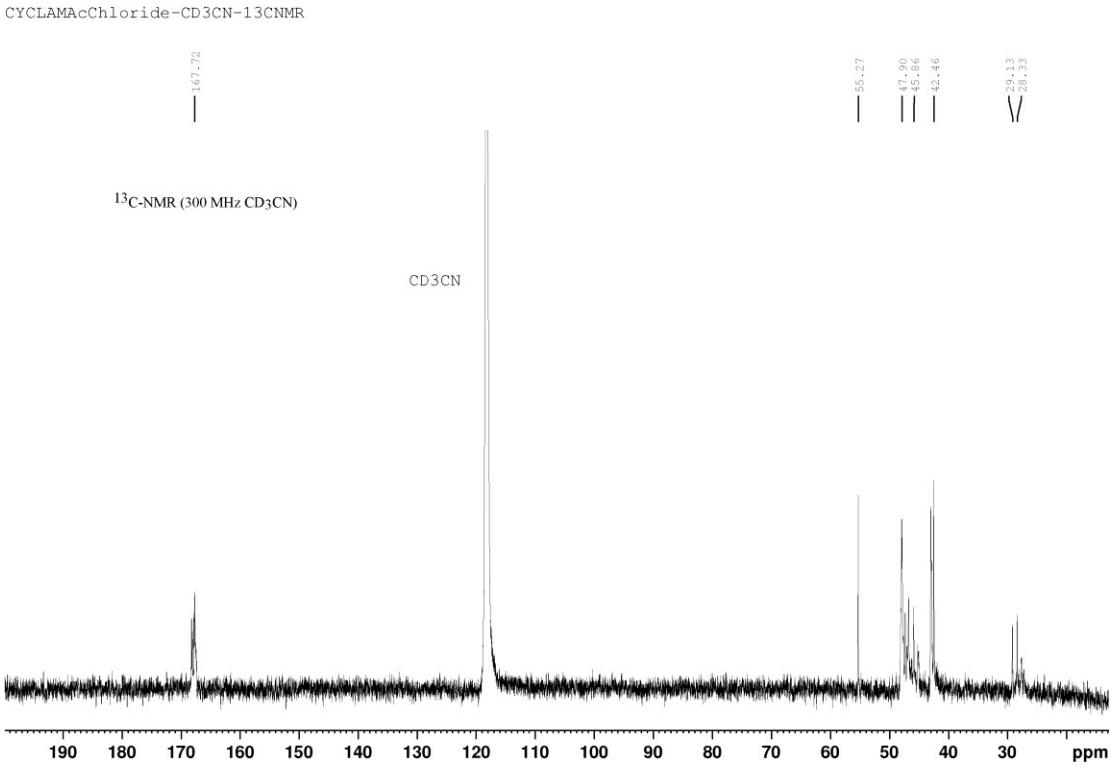

Data Set 2.1.3: FT-IR of solid CyclamAcCl collected at 298 K on Thermo Scientific, Nicolet iS5 (iD7-ATR)

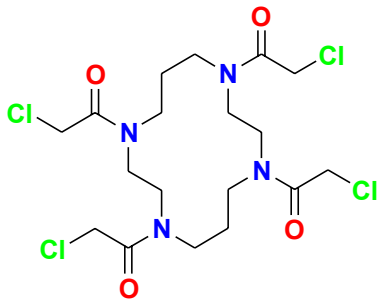

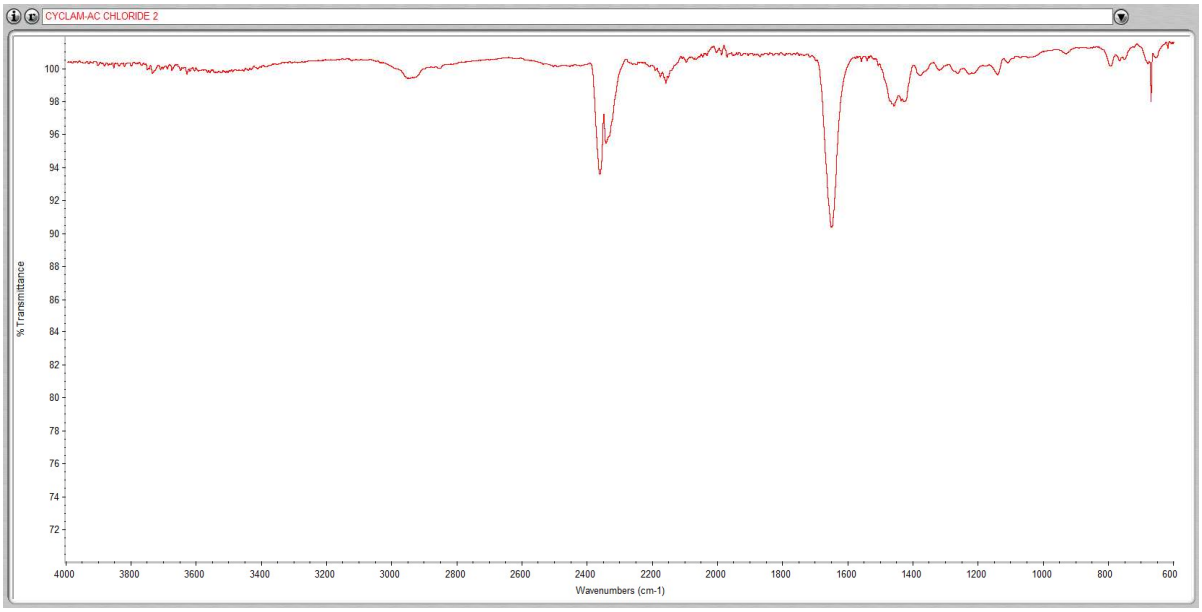

Data Set 2.1.4: LCMS of CyclamAcCl

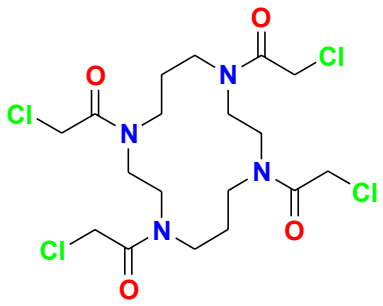

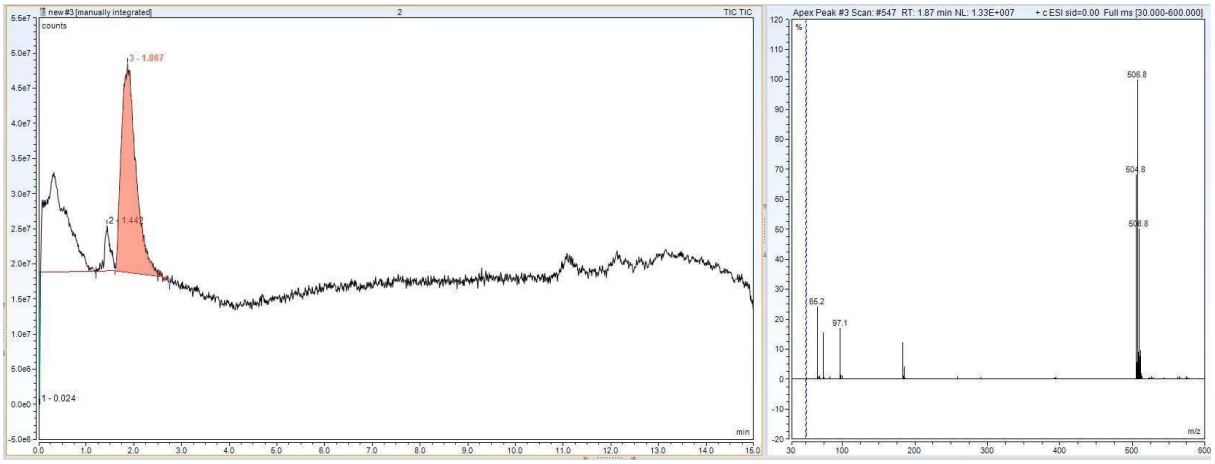

Data Set 2.2.1: ^{1}H-NMR of CyclamAcDPA recorded in $CDCl_3$ at 298 K

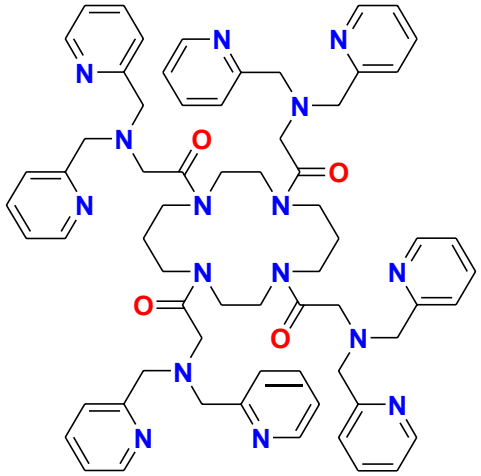

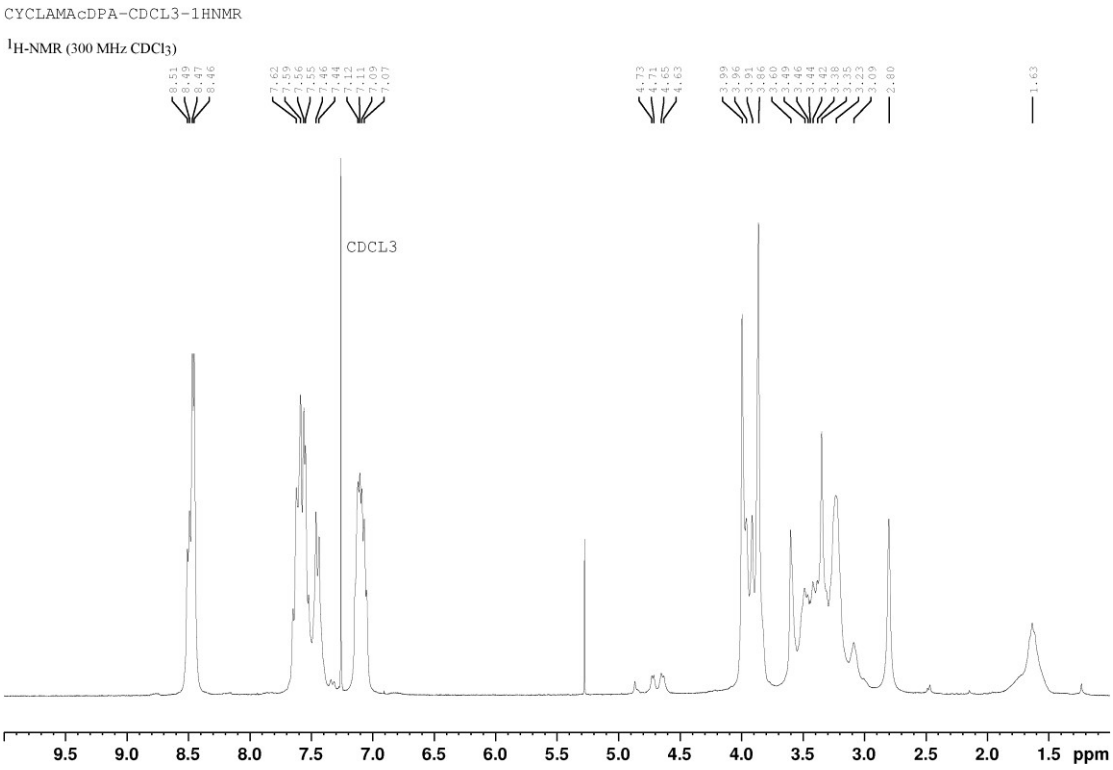

Data Set 2.2.2: ^{13}C-NMR of CyclamAcDPA recorded in $CDCl_3$ at 298

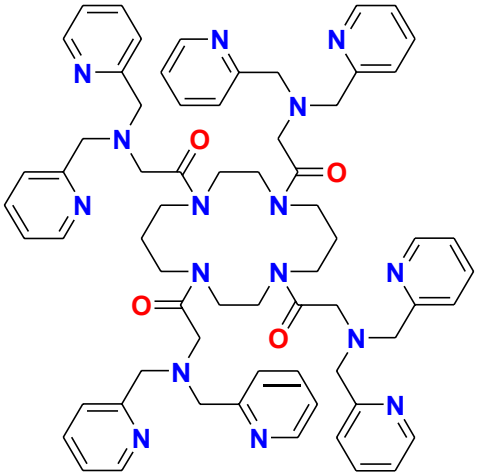

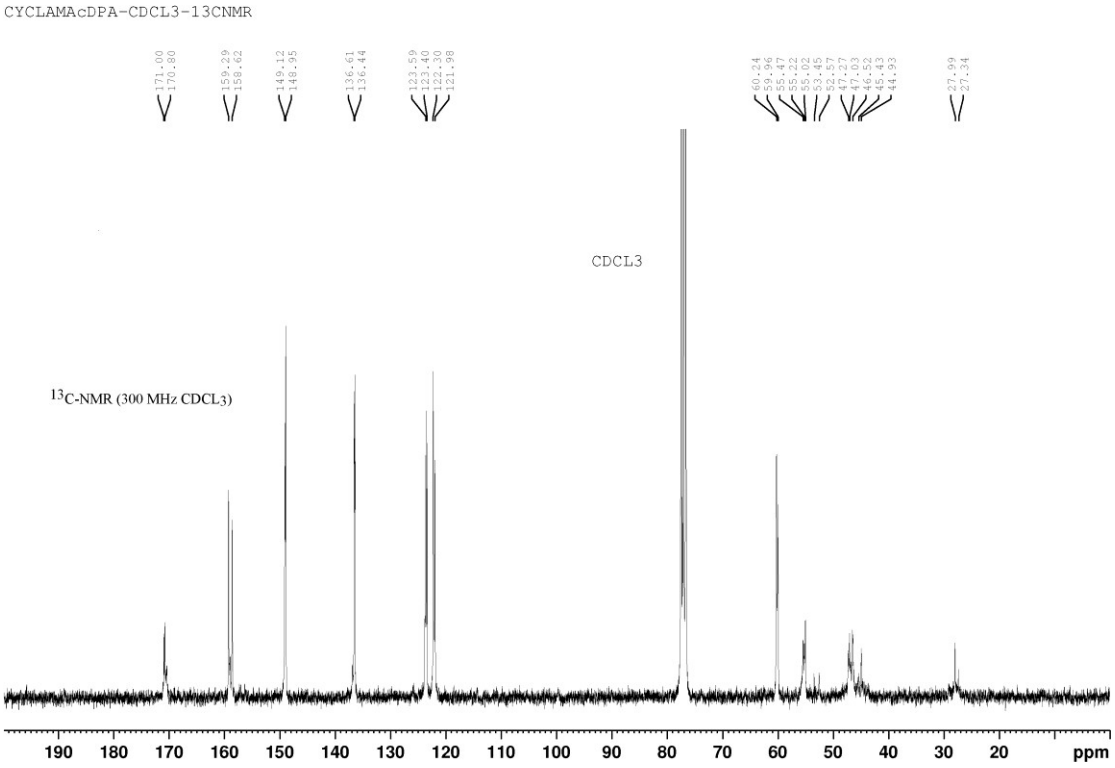

Data Set 2.2.3: FT-IR of CyclamAcDPA collected at 298 K on Thermo Scientific, Nicolet iS5 (iD7-ATR)

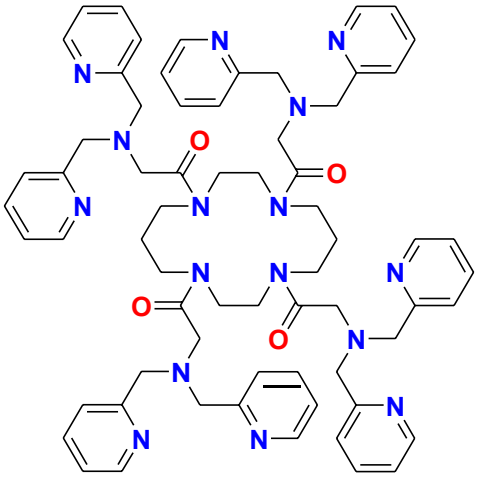

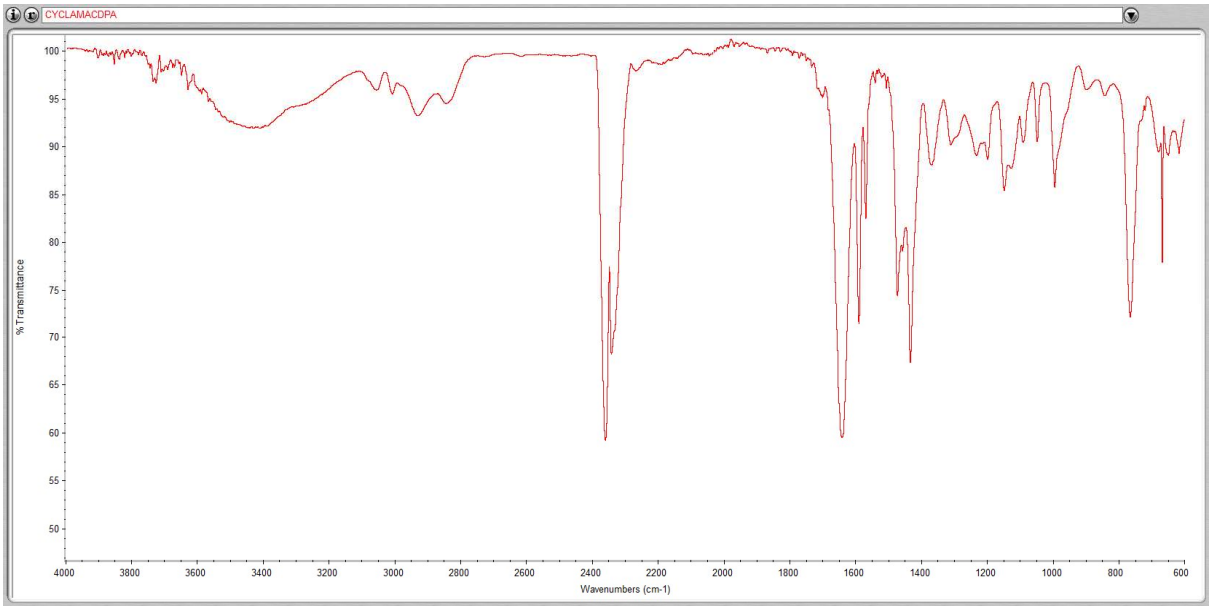

Data Set 2.2.4: LCMS of CyclamAcDPA

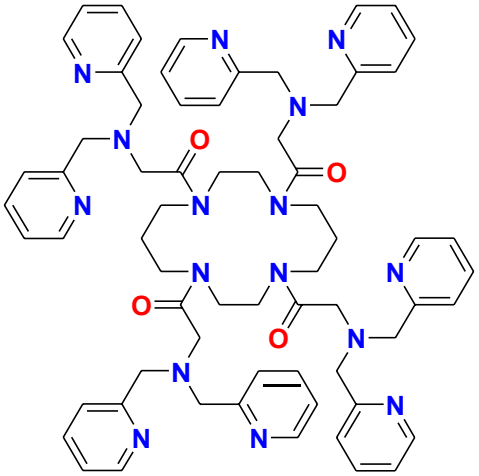

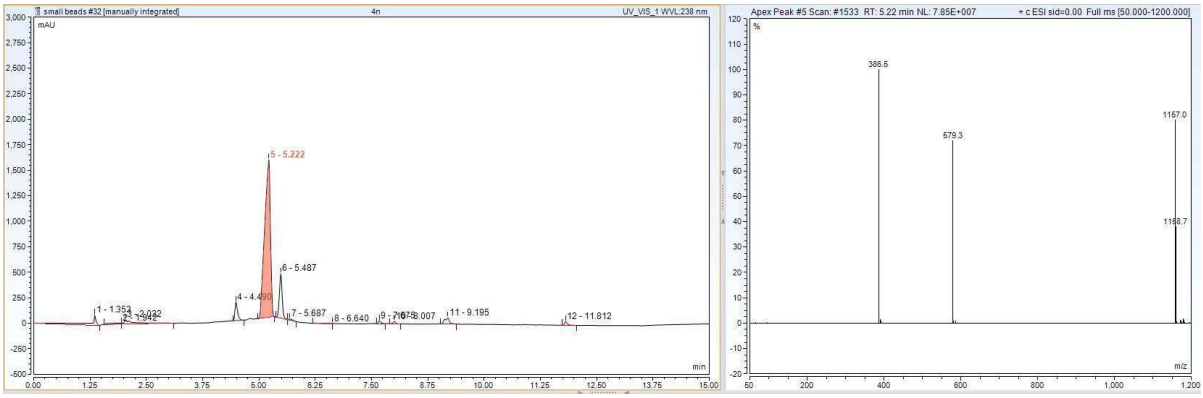

Data Set 2.3.1: ^{1}H-NMR of Mn(II)$_4$(L)(OTf)$_8$, L = CyclamAcDPA recorded in CD$_3$CN at 298 K

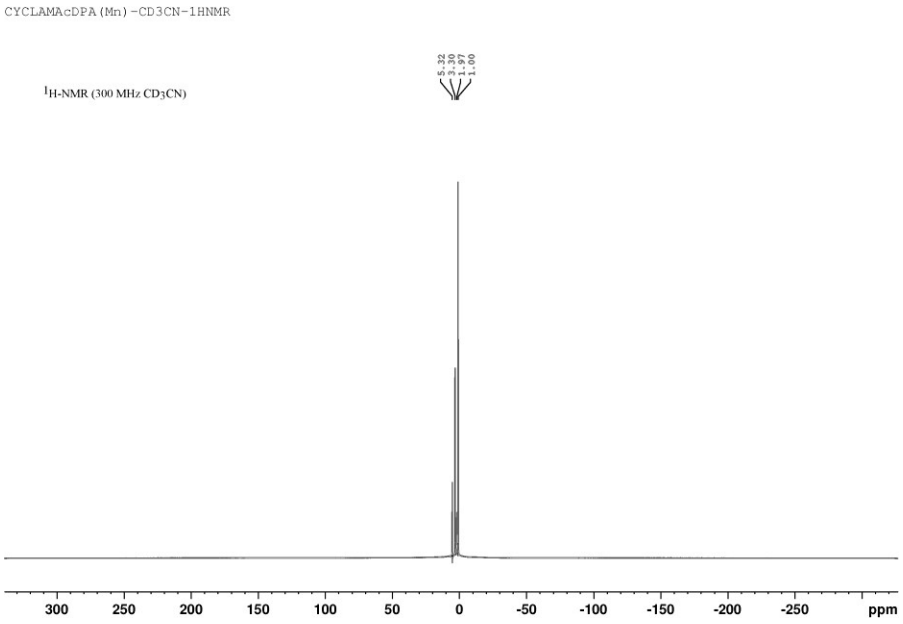

Data Set 2.3.2: UV-Vis absorption spectrum of Mn(II)$_4$(L)(OTf)$_8$, L = CyclamAcDPA recorded in CH$_3$CN at 298 K

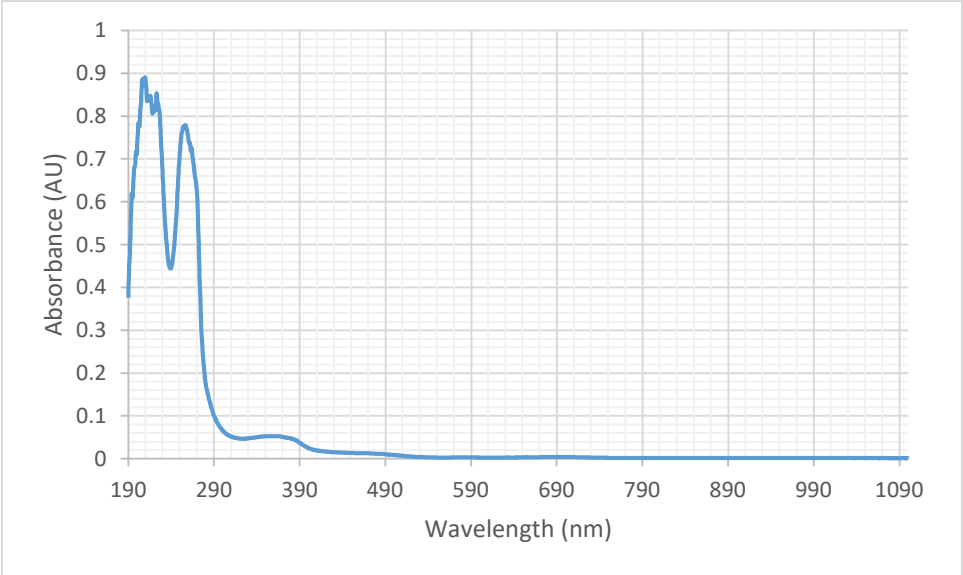

Data Set 2.3.3: FT-IR of solid $Mn(II)_4(L)(OTf)_8$, L = CyclamAcDPA collected at 298 K on Thermo Scientific, Nicolet iS5 (iD7-ATR)

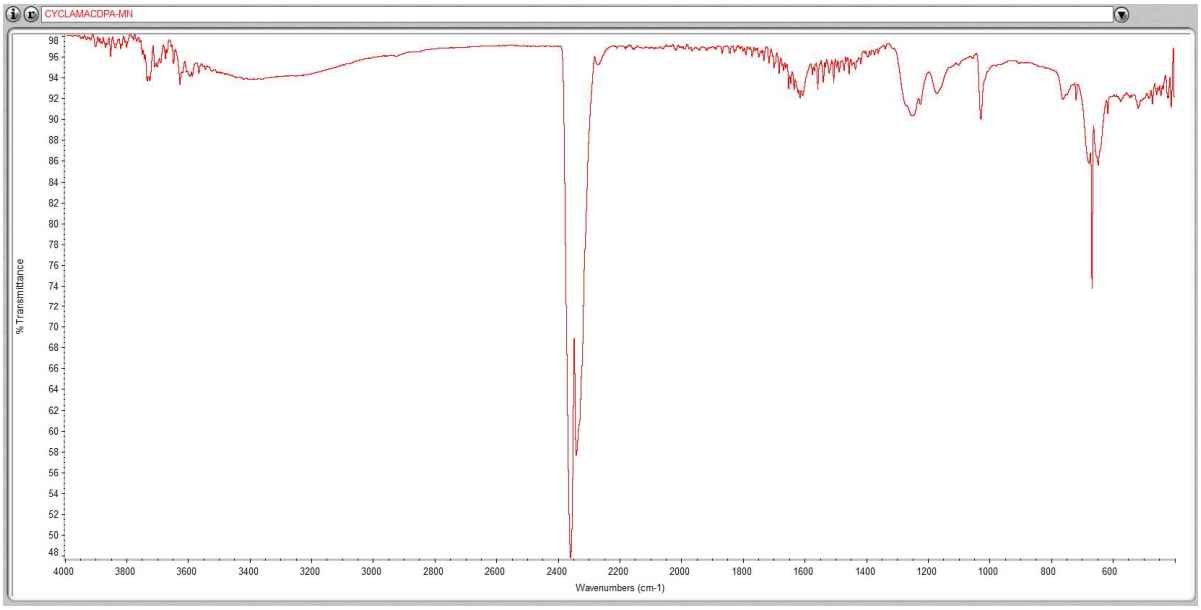

Data Set 2.4.1: ^{1}H-NMR of $Fe(II)_4(L)(OTf)_8$, L = CyclamAcDPA recorded in CD_3CN at 298 K

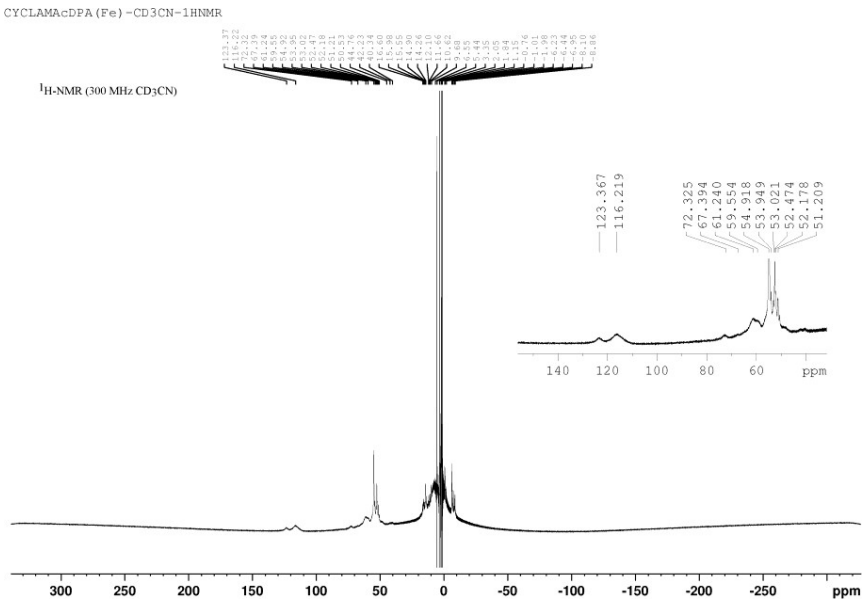

Data Set 2.4.2: UV-Vis absorption spectrum of $Fe(II)_4(L)(OTf)_8$, L = CyclamAcDPA recorded in CH_3CN at 298 K

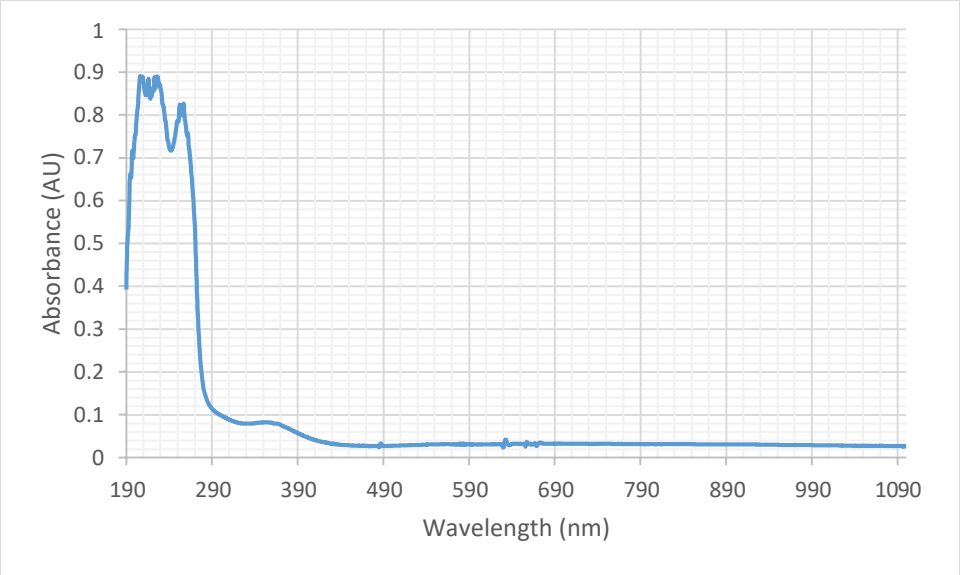

Data Set 2.4.3: FT-IR of solid $Fe(II)_4(L)(OTf)_8$, L = CyclamAcDPA collected at 298 K on Thermo Scientific, Nicolet iS5 (iD7-ATR)

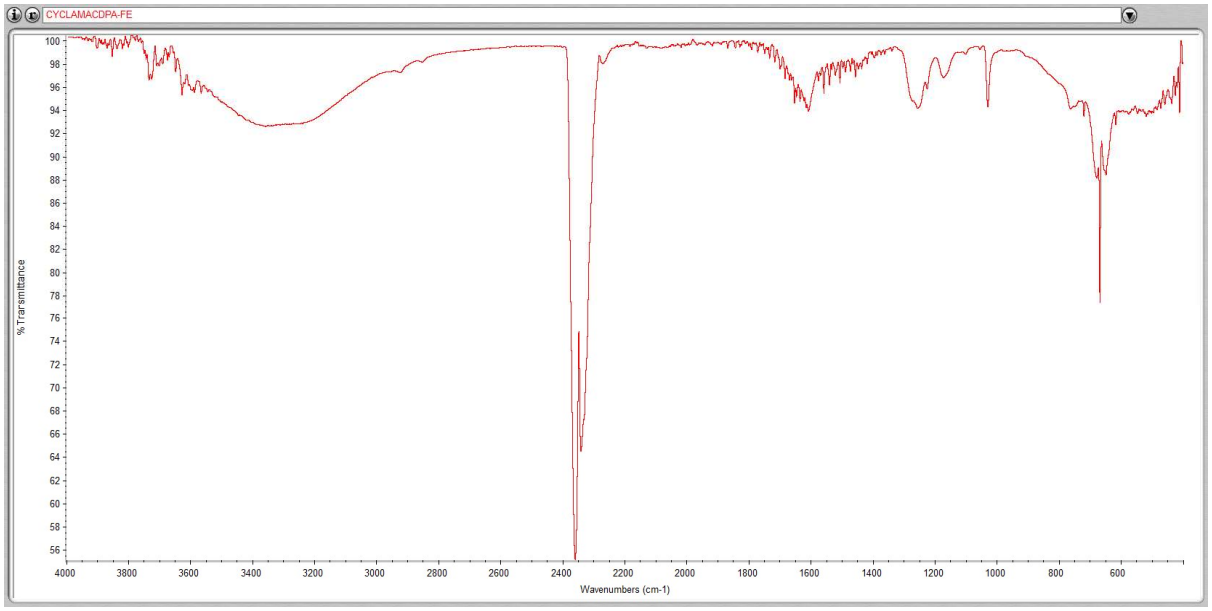

P.I. – Dr. Jai Prakash
Graduate Thesis by – Michael Kayne
Texas A&M University – Corpus Christi
2018 – 2020